N

Nanoionics at High Temperatures

J. Maier
Max Planck Institute for Solid State Research, Stuttgart, Germany

While in the bulk of materials local electroneutrality has to be fulfilled, at interfaces space charge zones occur which provide additional degrees of freedom defined by the contact chemistry. So it is the *individual* preference of a given charge carrier for a certain phase or the boundary core itself that is to the fore. The trade-off of this additional flexibility is the occurrence of an electrical field which confines the effects to the immediate vicinity of the interface.

In the case of crystalline solids, the calculation of the equilibrium charge carrier concentration as a function of the control parameters (typically partial pressures of the components, dopant concentration, and temperature) requires mass action laws of point defect generation or interaction, but in addition to these chemical constraints also an electrostatic constraint. In the bulk this is local electroneutrality, while at the boundaries excess charges can be tolerated but regulated by Poisson's equation and the respective boundary conditions. This excess charge decays to zero towards bulk within a characteristic length that typically is in the range of nanometers (maximum, about 100 nm for very pure materials; minimum, interatomic distance). Thus at interfaces, depending on the chemistry there, charge carriers can be accumulated or depleted by orders of magnitude compared to the bulk. Notwithstanding structural changes that might occur as well, this space charge effect occurs even and in particular for an abrupt junction. For surfaces of solids this has been addressed by Frenkel, Kliewer, and Blakeley [1–3]. A general treatment of space charge effects at interfaces as a function of the thermodynamic parameters and hence implementation in the defect chemical consideration was given by the author [4]. It is the latter procedure that paved the way for a systematic exploitation of space charge effects ("Heterogeneous Doping" or "Higher-dimensional Doping") with respect to materials design [5].

Figure 1 is a key figure in this context and highlights for a Frenkel-disordered solid the thermodynamic behavior of mobile electronic and ionic carriers at boundaries and their coupling [6]. Figure 2 is equally important as it shows the complete problem set to be solved using the example of surface space charges [7]. Based on this treatment it was possible to explain a great variety of anomalies as well as to predict and verify new systems of interest.

Figure 3 gives a collection of prototypes [8].

To emphasize the potential of this "higher-dimensional doping," let us consider a pure material in which cation vacancies and cation interstitials represent the relevant ionic carriers and in which the electronic carriers are in minority. Let us further imagine we are primarily interested in the cation vacancy owing to higher mobility. If the counter defect possesses a higher

G. Kreysa et al. (eds.), *Encyclopedia of Applied Electrochemistry*, DOI 10.1007/978-1-4419-6996-5,

defect formation energy than the cation vacancy, the cation vacancy concentration is very limited owing to electroneutrality irrespective of its quite favorable individual formation energy. A well-known remedy is (homogeneous) doping: in the special case considered, one would try to introduce a positively charged dopant. The benefits are very limited if the solubility for the dopant is small. If one, however, creates a situation where the metal ion is absorbed or adsorbed owing to the second phase or the core region of the contact (e.g., grain boundary core), metal vacancies are accumulated in the space charge zones of the material under concern. This accumulation effect can be huge but is restricted to the very surroundings of the contact. For properties that directly probe the interfacial situation (e.g., surface kinetics in fuel cells, electrochemical transfer reactions), this is immediately of great relevance. As far as overall transport properties are concerned, a high density of percolating interfaces is required for a substantial overall effect. Should the spacing of the interfaces be so small that the material is charged everywhere, then mesoscopic situations are realized.

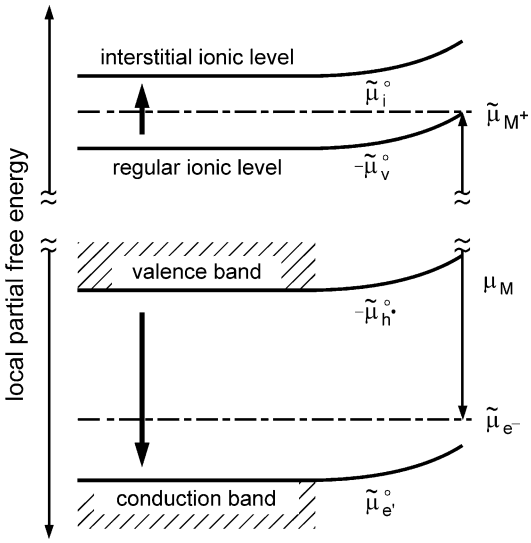

Nanoionics at High Temperatures, Fig. 1 The figure shows the energy level diagram for a mixed conductor MX with Frenkel disorder in the cation sublattice. *Top*: ionic disorder. *Bottom*: electronic disorder. The connection occurs via the chemical potential of the component (Reprinted from Ref. [6] by permission of Elsevier)

A thorough theoretical treatment together with various verified examples can be found in previous works of the author [4–9]. It is particularly important to note that all carriers that are mobile feel the field effect even if their contribution to it is marginal (fellow traveler effect) [4]. For that reason ionic space charge effects are also crucial for electronic conductors.

In the following, and referring to Fig. 3, a few characteristic situations are described that are of interest for high-temperature defect chemistry (see Ref. [10] and references therein):

1. A phenomenon of great practical relevance is the increase of ion conductivity by adding second surface active particles (a). The earliest example was LiI:Al_2O_3, [11] later examples are silver, copper, and thallium halides which showed similar effects [4, 5]. Similar effects can also be observed for anion conductors examples (e.g., PbF_2: SiO_2) (b) [4]. They all find their explanation in the concept of

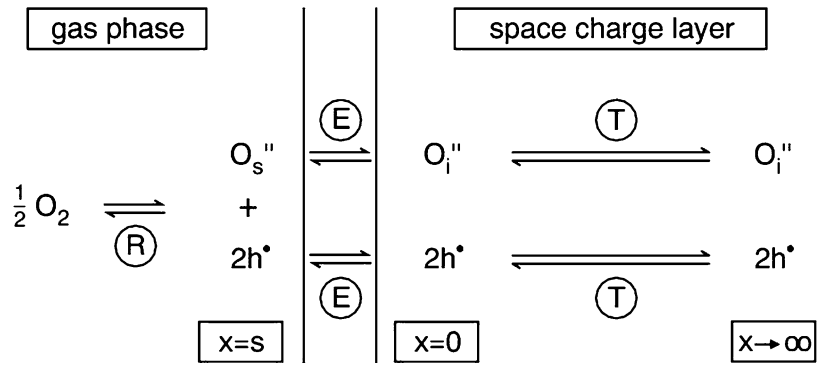

Nanoionics at High Temperatures, Fig. 2 Defect chemistry at a surface layer. Unlike $x \geq 0$, the ground structure is changed at $x = s$ (referring to the surface or adsorption layer) (Reprinted from Ref. [7])

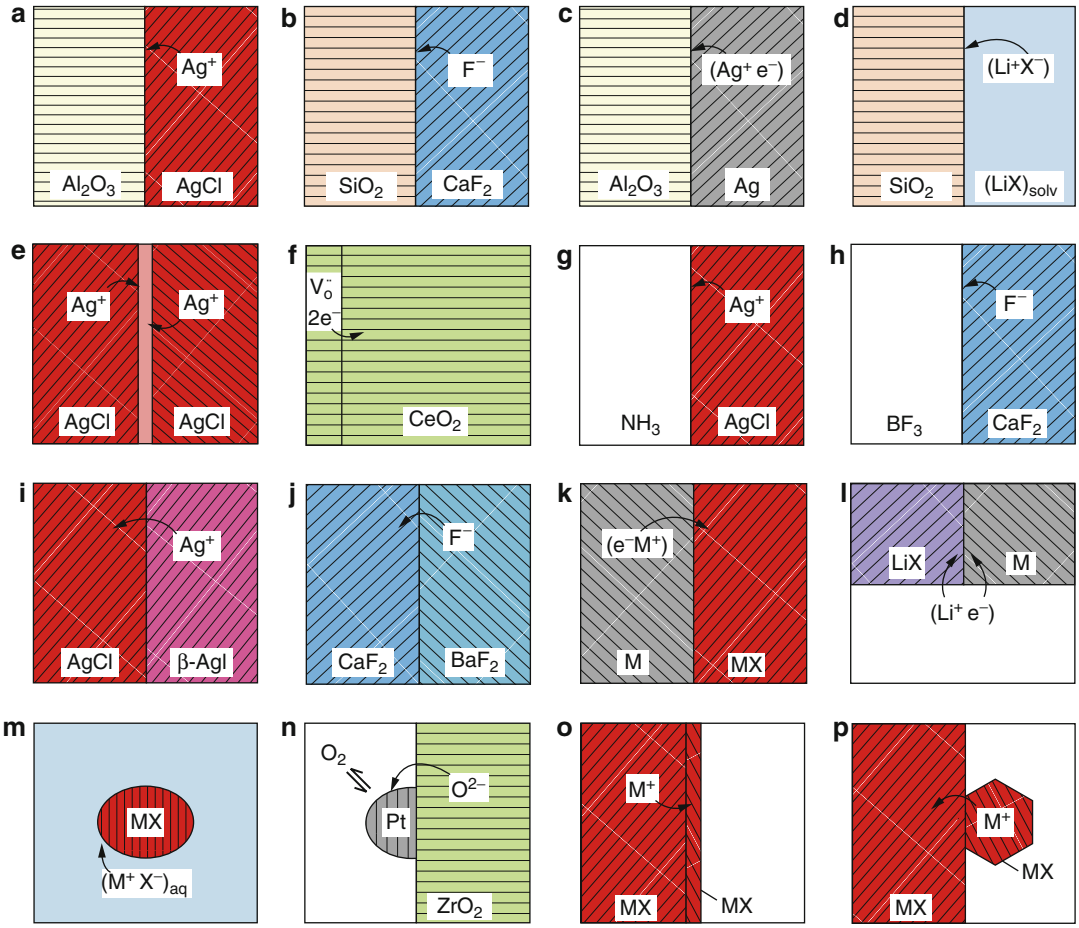

Nanoionics at High Temperatures, Fig. 3 A collection of ionic space charge effects at interfaces involving solids (Reprinted from Ref. [8] by permission of Elsevier)

heterogeneous doping, as quantitatively developed in Refs. [4–10,12].

A key parameter is the point defect concentration (c_0) directly adjacent to the interfacial core containing the information on the second phase. From a thermodynamic viewpoint, we better express c_0 in terms of surface charge density or even better in terms of the "energy levels" as the real invariants (see Fig. 1) [12].

2. Space charge zones also occur at surfaces. Exciting examples are Ag-halide surfaces the excess charge of which can be varied by acid–base active gases (g). This can be nicely exploited for chemical sensing of acid–base active gases such as NH_3. (The anionic analogue to NH_3: AgCl is BF_3: CaF_2 [5].) Other examples of interest are stoichiometry and lattice constant anomalies in CeO_2 [13, 14].
3. If the second phase is a Frenkel-disordered ionic conductor itself, Ag^+ can be absorbed and accommodated in its charge zones, rather than just adsorbed. Examples are AgI: AgBr, AgI: AgCl (i), or CaF_2: BaF_2 as anionic counterpart (j) where ions can redistribute in addition to possible neutral mixing demanded by the phase equilibrium. A particularly thorough study referred to CaF_2/BaF_2 heterolayers as here the morphology is simple and the layer thickness could be varied from nm to μm. The situation becomes exciting if the thickness of

the layers is so small that the space charge zones overlap, then not a single point within the layers remains electroneutral [15].

4. Excess charges also occur in polycrystalline materials owing to charging of the interfacial core. So in Ag-halides (i) or BaF_2, CaF_2 (j), we find Ag^+ or F^- accumulation in the core and vacancy accumulation in the space charge zones. This effect can be chemically augmented by contaminating the grain boundaries with Lewis acids or bases [5]:

   In oxide systems [16–22] the grain boundary core is often found positively charged owing to ex-corporation of O^{2-} in order to energetically stabilize the grain boundary. This positive core charge leads to a variety of significant phenomena (see Fig. 4): depletion of holes resulting in an increased resistance of p-type $SrTiO_3$, even greater depletion of oxygen vacancies. The increase of excess electrons is most clearly seen in CeO_2 where lightly doped CeO_2 switches from ion to electron conductivity if downsized. Depletion of protons in oxidic materials appears to be the reason for the enormous grain boundary resistances in $BaZrO_3$ preventing the material from being an excellent proton conductor in polycrystalline form. The joint effects on excess electrons; holes and oxygen vacancies can be nicely seen in the oxygen partial pressure dependence of the transport properties in nanocrystalline $SrTiO_3$. Also here the grains are in the mesoscopic regime. As far as the electronic contribution is concerned, downsizing to about 30 nm leads to a change in the electronic defect chemistry that is equivalent to a P_{O2} change of 12 orders of magnitude. The ionic contribution essentially vanishes (depression by 6 orders of magnitude) [23].
5. As point defects are also highly reactive centers, the space charge in particular at surfaces is very important for heterogeneous catalysis [24–26]. A few studies are available that highlight the significance of heterogeneous doping in that respect. Related effects that also rely on charging and the individual redistribution of ions are spillover and the variation of catalytic activity by polarizing a solid electrolyte (h) [24, 27].

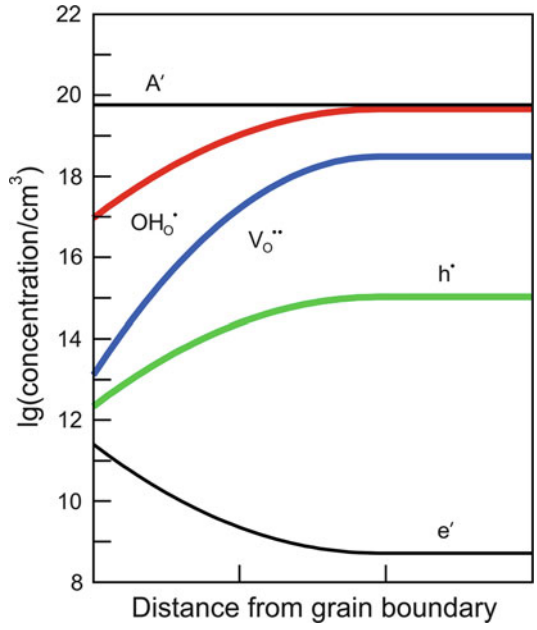

Nanoionics at High Temperatures, Fig. 4 Carrier concentrations near a positively charged grain boundary core in oxide systems (here: Mott-Schottky situation in an acceptor (A') doped oxide)

6. A related area in which now experiments are underway is the significance of space charge zones for chemical or electrochemical reactions at surfaces or interfaces. Large effects are expected as the relevant interfacial carrier concentration is greatly affected (surface vacancies).
7. Space charge zones can also lead to storage anomalies, as shown recently in the context of Li-based batteries (l). As described in Ref. [28], early results [29, 30] on greatly varied miscibilities in the system (Ag-chalcogenide: Al_2O_3) may be explained in this way. Similarly one has to reckon with varied (charged) non-stoichiometries at oxide interfaces. This list can be prolonged, in particular as phenomena at lower temperature are concerned.

These selected master examples highlighted the significance of nanoionics for applied electrochemistry as to find better electrodes, electrolytes, catalysts, and chemical sensors. It is also a fundamentally exciting area, as it leads to (i) new mechanisms and (ii) to new adjusting

screws. In addition to temperature component partial pressure and doping content, these new degrees of freedom are nature, density, and distribution of interfaces and hence include size effects.

A key point which is heavily investigated at the moment is how to influence and tune the core charge of given systems. Whether or not this will work out satisfactorily, it can be foreseen that nanoionics will play a similarly important role for energy research as nanoelectronics does for information technology.

So far the ionic space charge concepts have been mainly applied to transport and storage. An area that is not adequately addressed but expected to be greatly influenced by such effects is the area of interfacial transfer and reactions including reaction kinetics, catalysis, or in particular the electrochemical transfer reaction. In many of these processes, defect concentrations are involved in the rate determining steps and not only will space charge considerations help understand them but more importantly lead to a targeted improvement of electrochemical performance.

Cross-References

► Solid Electrolytes

References

1. Frenkel J (1926) Thermal movement in solid and liquid bodies. Z Physik 53:652–669
2. Kliewer KL, Koehler JS (1965) Space charge in ionic crystals. I. General approach with application to NaCl. Phys Rev A 140:1226–1240
3. Poeppel RB, Blakely JM (1969) Origin of equilibrium space charge potentials in ionic crystals. Surf Sci 15:507–523
4. Maier J (1987) Defect chemistry and conductivity effects in heterogeneous solid electrolytes. J Electrochem Soc 134:1524–1535
5. Maier J (1995) Ionic conduction in space charge regions. Prog Solid State Chem 23:171–263
6. Maier J (2003) Defect chemistry and ion transport in nanostructured materials. Part II. Aspects of nanoionics. Solid State Ion 157:327–334
7. Maier J (2004) Physical chemistry of ionic materials. Ions and electrons in solids. Wiley, Chichester
8. Maier J (2004) Ionic transport in nano-sized systems. Solid State Ion 175:7–12
9. Maier J (1987) Space charge regions in solid two phase systems and their conduction contribution-III: defect chemistry and ionic conductivity in thin films. Solid State Ion 23:59–67
10. Maier J (2009) Nanoionics: ionic charge carriers in small systems. Phys Chem Chem Phys 11:3011–3022
11. Liang CC (1973) Conduction characteristics of lithium iodide aluminium oxide solid electrolytes. J Electrochem Soc 120:1289–1292
12. Jamnik J, Maier J, Pejovnik S (1995) Interfaces in solid ionic conductors: Equilibrium and small signal picture. Solid State Ion 75:51–58
13. Kim S, Merkle R, Maier J (2004) Oxygen nonstoichiometry of nanosized ceria powder. Surf Sci 549:196–202
14. Kossoy A, Feldman Y, Wachtel E, Gartsman K, Lubomirsky I, Fleig J, Maier J (2006) On the origin of the lattice constant anomaly in nanocrystalline ceria. Phys Chem Chem Phys 8:1111–1115
15. Sata N, Eberman K, Eberl K, Maier J (2000) Mesoscopic fast ion conduction in nanometre-scale planar heterostructures. Nature 408:946–949
16. Denk I, Claus J, Maier J (1997) Electrochemical Investigations of SrTiO3 Boundaries. J Electrochem Soc 144:3526–3536
17. Balaya P, Jamnik J, Fleig J, Maier J (2006) Mesoscopic electrical conduction in nanocrystalline SrTiO3. Appl Phys Lett 88:062109
18. De Souza RA, Fleig J, Maier J, Kienzle O, Zhang Z, Sigle W, Rühle M (2003) Electrical and structural characterization of a low-angle tilt grain boundary in iron-doped strontium titanate. J Am Ceram Soc 86:922–928
19. Tschöpe A (2001) Grain size-dependent electrical conductivity of polycrystalline cerium oxide II: Space charge model. Solid State Ion 139:267–280
20. Chiang YM, Lavik EB, Kosacki I, Tuller HL, Ying JY (1996) Defect and transport properties of nanocrystalline CeO_{2-x}. Appl Phys Lett 69:185–187
21. Kim S, Maier J (2002) On the conductivity mechanism of nanocrystalline ceria. J Electrochem Soc 149 (10): J73–J83
22. Shirpour M, Lin CT, Merkle R, Maier J (2012) Nonlinear electrical grain boundary properties in proton conducting Y-$BaZrO_3$ supporting the space charge depletion model. Phys Chem Chem Phys 14:730–740
23. Lupetin P, Gregori G, Maier J (2010) Mesoscopic charge carriers chemistry in nanocrystalline $SrTiO_3$. Angew Chem Int Ed 49:10123–10126
24. Fleig J, Jamnik J (2005) Work function changes of polarized electrodes on solid electrolytes. J Electrochem Soc 152: E138–E145
25. Murugaraj P, Maier J (1989) Heterogeneous catalysis with composite electrolytes. Solid State Ion 32/33:993–999

26. Merkle R, Maier J (2006) The significance of defect chemistry for the rate of gas-solid reactions: three examples. Topics Catal 38:141–145
27. Riess I, Vayenas CG (2003) Fermi level and potential distribution in solid electrolyte cells with and without ion spillover. Solid State Ion 159:313–329
28. Maier J (2007) Mass storage in space charge regions of nano-sized systems (Nano-ionics. Part V). Faraday Discuss 134:51–56
29. Petuskey WT (1986) Interfacial effects on Ag: S nonstoichiometry in silver sulfide/alumina composites. Solid State Ion 21:117–129
30. Janek J, Mogwitz B, Beck G, Kreutzbruck M, Kienle L, Korte C (2004) The magnetoresistance of metal-rich Ag2+xSe - A prototype nanoscale metal/semiconductor dispersion? Prog Solid Sate Chem 32:179–205

Neural Stimulation Electrodes and Sensors

J. Thomas Mortimer
Case Western Reserve University,
Cleveland, OH, USA

Introduction

The electrical excitability phenomenon, inherent to neural tissues, provides an opportunity to effect external control over many body systems: paralyzed limbs can be made to move, the blind can experience visual sensations, the deaf people can experience the voice of others close by or by phone, pain can be alleviated, tremors suppressed, and mental disorders treated. Devices, often referred to as neuroprostheses, that perform these functions can be sold. Companies that make devices that provide the most function with the smallest, safest devices that also have long battery lifetimes usually have the market advantage. Function is directly related to electrode placement; improperly placed electrodes don't work or have undesirable side effects. The remedy has been reimplantation, but tunable electrodes, structures with multiple small contacts, are making it possible to avoid additional surgery by providing pathways to manipulate the shape of the excitatory fields. Device size is often dictated by the size of the battery, and the body usually accommodates smaller devices more easily. Safe devices don't cause tissue injury. Devices that have long battery life don't require replacement as often. On the down side, devices do fail and inject unintended charge through the electrode contacts causing changes local to the contact site that often lead to costly litigation. Life-changing experiences are opened with these devices, and money can be made and lost. Understanding how they work or made to work more efficiently is key to their growing use and success. Further, bringing new devices or improved devices to the market can involve costly animal trials because of safety concerns. Electrical charge, weather drawn from internal batteries or injected through metal contacts into the electrolytes found in the living system, is common to understanding and improving neural prostheses.

It should come as no surprise to an electrochemist that many of these issues reduce to injecting the least amount of charge with the least amount of electrical potential to get the job done. Minimizing the amount of charge injected lessens the drain on power sources and lessens the likelihood that bad things will happen at the electrode-electrolyte interface where the target cells live. Keeping the potential low, particularly the ohmic losses, usually means the battery is physically smaller for the implantable pulse generator.

Typically neural stimulating electrodes:

- Are platinum or stainless steel in commercially available devices.
- Subjected to current densities that can be in the range of 1 A/cm^2.
- Employ pulse configurations that are biphasic with the cathodic phase first.
- See pulse durations range from 50 to 200 μS, with lower and higher values also employed and are subjected to.
- Repetition rates range from 10 to 200 Hz with higher rates used in some applications.

The job to be done by an electrode, connected to a current or potential source, is to create a potential field in the region of neural tissues that is capable of initiating a propagated action

potential. The propagated action potential is a signal traveling on a unity-gain transmission line, the axon or nerve fiber, from the signal source, usually the cell body of the nerve or neuron, to the terminal end where the invading potential change initiates the release of a neurotransmitter, transferring the signaling information to the target cell, e.g., muscle or another neuron. Basically, the axon is the means by which the brain receives information and gives commands to and receives commands from distant parts of the body. The unity-gain feature of the axon is the phenomenon we harness to take control of the nervous system.

Basics of the Stimulation Target, the Axon

Information is carried in the nervous system by pulsed signals carried on axons designated for specific functions, e.g., vision, hearing, pain, and limb movement. Usually a higher pulse repetition rate implies a more intense piece of information being transmitted, and often bursts are used to get the attention of certain cells. Repetition rates, sometimes called firing rates, run in the range of 10 Hz to a couple of 100 Hz, with some body systems operating above, for short periods, and below these values. The firing rate determines the nature of the transmitter released at the terminal end, which is the key information transferred.

The neural signal is a localized transient change in the transmembrane potential of the axon (each less than 20 μm in diameter). The unity-gain transmission is achieved by having repeaters spaced along the axon at distances below 2 mm over the entire length. The repeaters are clusters ($\sim$1,000 per μ^2) of voltage-gated sodium ion channels isolated to the nodes of Ranvier, the gap between cells acting to insulate the length of the axon. The resting membrane potential is maintained at or near the Nernst potential for potassium by voltage-gated potassium ion channels, allowing potassium to move from inside to outside the membrane. Depolarization, sodium moving from outside to inside the cell, of one node creates a potential difference between nodes and initiates the depolarization of adjacent nodes, which accounts for the propagation of the signal. Movement of potassium from the inside to the outside of the membrane reestablishes the resting membrane potential in preparation for the next signal to be transmitted.

Stimulation-Induced Action Potentials

When a current or voltage pulse is applied to an electrode in a living system, double-layer charging takes place and if the potential is sufficient electron transfer occurs across the electrode-tissue interface. Further away from the interface ions move, in response to the local changes, to the induced by the current injected into the electrode and create a spatial potential gradient, and if that area contains axons, action potentials can be initiated that propagate the entire length of the axon as if they were naturally initiated.

Strength-Duration Curve: Shorter Duration Pulses Require Larger Amplitudes

When the electrical excitability phenomenon of axons was discovered, investigators explored the relationship between pulse duration and pulse amplitude required to initiate an action potential on an axon. The results of their investigation looked something like the graph shown in Fig. 1a, which indicates that larger currents are required to initiate an action potential when shorter pulse durations were used. In order to account for the fact that the separation between the electrode and the excitable tissues determined the magnitude of the stimulus, the term rheobase current (I_r) was defined as the asymptote defining the minimum current and the chronaxie time (t_c) was the time defined by the point on the duration axis at twice the rheobase current. The chronaxie time is relatively stable from lab to lab and measurement to measurement for given tissues where as the rheobase is variable.

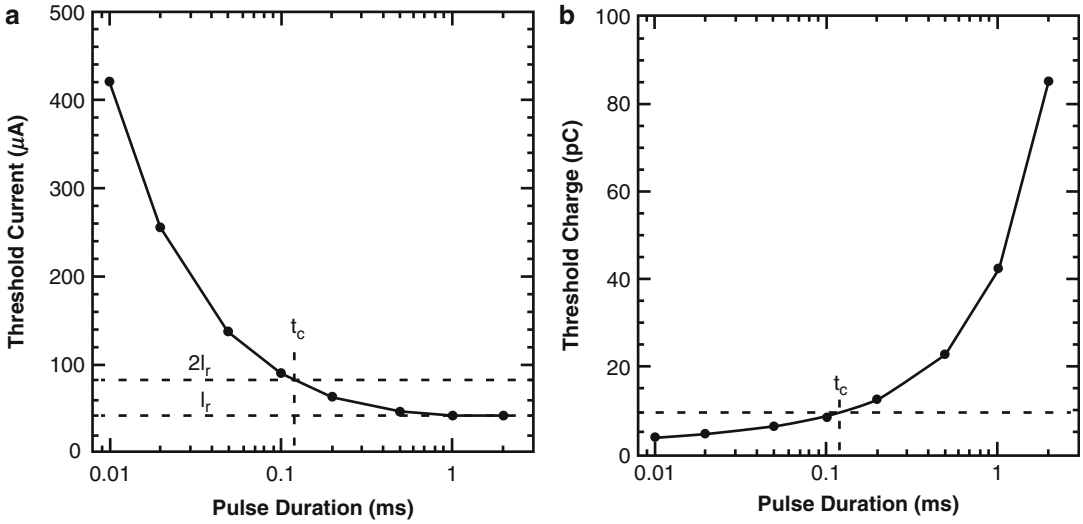

Neural Stimulation Electrodes and Sensors, Fig. 1 Strength-duration (**a**) and charge-duration (**b**) plots for nerve stimulation [1]. The current amplitude required to create a propagated action potential has been experimentally found to increase as the duration of the current pulse decreases. The actual magnitude depends on the separation between the electrode and nerve, which shifts the plot shown in **a** up or down. To accommodate for the shift and to make the result from one laboratory useful to another laboratory, the rheobase current is defined as the minimum current for a very long pulse, the asymptote. Doubling this value, $2I_r$, and measuring the intersection with the experimentally derived data defines the chronaxie time (t_c), a measurement easily transferable between laboratories. The chronaxie for neural tissue is in the range of 100 μS and the chronaxie for muscle tissue is in the range of 10 mS. Multiplying the current amplitude in **a** by the pulse duration yields the charge delivered to the nerve. Plotting the charge as a function of pulse width produces **b**. In **b** it is noted that the injected charge, required to effect a propagated action potentials, decreases with decreasing pulse width

Charge-Duration Curve: Short Duration Pulses Are More Efficient

The relationship between charge injection required to initiate a propagated action potential and the pulse duration can be found by reformulating Fig. 1a into a charge-duration curve (Fig.1b). We learn from this plot that charge required to initiate a propagated action potential decreases with decreasing pulse width and to minimize the amount of charge injected, one should use the shortest possible pulse width. Practical constraints are brought to bear when one actually builds a stimulator because of power supply considerations (Fig. 1a). Generally speaking, pulse durations in the range 50–200 μS are used in most electrical stimulation devices, right around the chronaxie.

Charge Injection Limits to Avoid Tissue and Electrode Damage

If target tissue is damaged or the electrode destroyed by a device with an intended purpose of restoring or providing a therapeutic effect the device fails, not good for many reasons. The mechanism for tissue damage is not now known. There are two schools of thought, (1) hyperactivity brought on by forcibly driving the target cells and (2) by toxic products of the charge transfer process. They are not mutually exclusive, but this author subscribes to the electrochemical aspect, which forces the focus on the metals used at the charge transfer site.

Platinum and stainless steel are two metals extensively used in commercially available implanted neurostimulating devices. Studies have

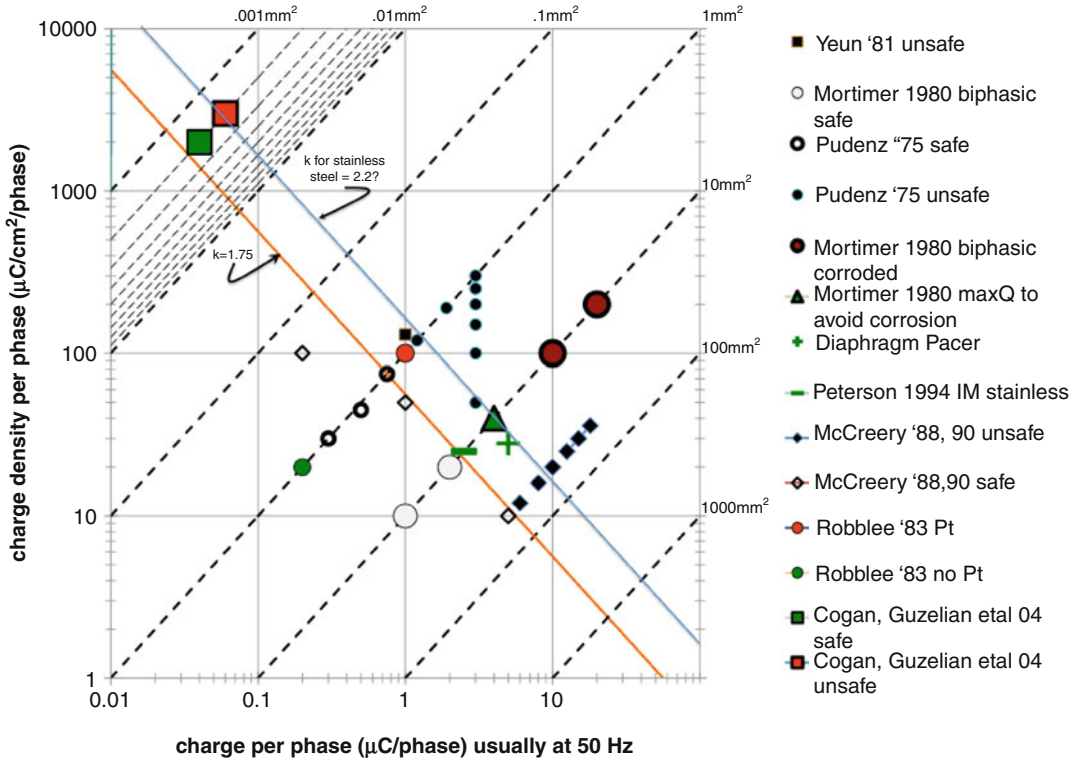

Neural Stimulation Electrodes and Sensors, Fig. 2 Shannon plot. This graph presents experimental data on safe and unsafe levels of stimulation. The safe and unsafe data are separable by the orange line defined by k = log (Q/A) + log (Q) and in this case k = 1.75. Charge and charge density values to the left of the line have been deemed safe from animal experiments using platinum electrodes applied to the brain, *small white filled symbols*, and values to the right have been deemed unsafe, *small black filled symbols*. The *small circles* indicate result where platinum was found in the brain tissue, *red filled*, and no platinum was found, *green filled*. The data appearing on the 10 mm^2 line (*dashed line* moving from *lower left* to *upper right*) are all for stainless steel electrodes in muscle. The safe values for stainless steel *white filled* or *green*. The *brown filled symbols* represent data from experiments in muscle where the electrodes were found to be corroded, but no significant tissue damage was observed. The *green filled triangle* depicts a point where the anodic corrosion potential limits maximum charge and charge density for a stainless steel electrode when charge balance is applied. The *green filled square* represents data collected from iridium oxide microelectrodes where the electrode appearance and tissue responses were deemed safe, and the *red filled* values represent electrode and tissue injury

been carried out with electrodes implanted in and on brain and muscle of animals and the tissues excised for microscopic analysis. The results of the early experiments using platinum electrodes were studied by Robert Shannon [2]. He found that plotting the results as log (charge per unit area) as a function of log (charge) yielded a plot where the "safe" and "unsafe" data could be separated by a line defined by:

$$k = logQ/A + logQ$$

There is no known explanation for these results, but they work and seem to apply to a range of electrode sizes.

Since Shannon's publication I have added experimental data to that plot; Shannon plot shown in Fig. 2 [3–10]. Consider first **platinum**: filled black symbols are data for levels deemed

"unsafe" for platinum electrodes applied to brain tissues, and open symbols are deemed "safe." The line defined as k = 1.75 separates the "safe" (lower left) and "unsafe" (upper right) platinum data. The dashed lines are lines of constant electrode area (geometric).

A designer will use this plot to specify maximum limits for stimulation. For example, say that a device has been designed with a platinum electrode having a geometric area of 1 mm^2. From the Shannon plot, the maximum "safe" limit for charge injection is 0.75 μC. For this electrode and for a 100 μs pulse, the maximum "safe" amplitude would be 7.5 mA or 0.75 A/cm^2.

Now consider stainless steel, usually 316 LVM. These electrodes were all formed by winding stainless wire, stranded and single strand, into a helix and inserting them, with the aid of a hypodermic needle, into muscle of cat. The area of the conducting surface was estimated to 10 mm^2. These data are presented in the Shannon plot as filled symbols plotted on the 10 mm^2 line [6]. The two white symbols represent data collected for balanced charge biphasic, cathodic first, pulses at 1 and 2 μC/phase, which were deemed safe. Increasing the charge injection to 10 and 20 μC/phase for balanced charge biphasic, cathodic first, pulses, brown filled symbols, caused the electrodes to corrode but did not cause an increase in muscle tissue damage. It was determined that at charge density less than or equal to 40 $\mu C/cm^2$ would not cause corrosion of the stainless steel electrodes, green filled triangle symbol. If Q/A(Q) for stainless steel has a similar relationship to that found for platinum, then the k value for stainless steel would be 2.2, meaning that more charge can be "safely" injected with stainless steel than platinum! These results put the charge injection limits on stainless steel as electrode corrosion rather than tissue damage. Subsequent experiments using *imbalanced biphasic* pulses [11], less charge in the anodic phase than the cathodic phase, demonstrated that charge densities as great as 120 $\mu C/cm^2$, threefold increase, could be "safely" applied to muscle without causing corrosion or tissue damage.

Speculation on the Cause of Tissue Damage with Platinum Electrodes

The data presented on stainless steel point to corrosion as the limiting factor, and the results indicate that cells in the immediate vicinity of the electrode can tolerate the corrosion products of stainless steel. Now, consider the two filled circle symbols for Robblee'83 data. The red filled symbol represents data where platinum was measured in the capsule and in the first millimeter of brain tissue at charge density injection rates of 100 $\mu C/cm^2$/phase AND; this datum point lies to the right of the k = 1.75 line! No platinum was detected in the capsule or the brain tissue for charge injection rates of 20 $\mu C/cm^2$/phase, a datum point to the left of the k = 1.75 line. These observations suggest that the corrosion products of platinum may be a causative factor.

In the 1960s Rosenberg was studying the role of electric currents on cell division and serendipitously discovered that cisplatin, a reaction product of the electrochemistry, was toxic to the cells in the culture [12]. The mechanism of toxicity is believed to be cisplatin interacting with DNA of the cell to induce programmed cell death, apoptosis [13]. Cisplatin has subsequently become a widely used anticancer agent, particularly for treating testicular cancer. In 1977 Agnew and colleagues [14] reported the results of injecting platinum salts into the brain of cats. They reported that the ultrastructural changes bore a likeness to the ultrastructural changes induced by electrical stimulation. It is curious that neither Robblee and her colleagues nor Agnew and his colleagues, all very familiar with neural stimulation of the brain, never acknowledged a connection to cisplatin.

Drawing from the stainless steel experience, if cisplatin, a product of platinum corrosion, occurs during electrical stimulation of the brain with platinum electrodes, it will be possible to increase the charge injection through platinum electrodes to values beyond k = 1.75 by using imbalanced biphasic pulses, less charge in the anodic phase. When balanced charge biphasic pulses are employed, any charge going into irreversible reaction products during the cathodic phase will

force the electrode potential positive to the potential prior to the initiation of the cathodic phase. When the electrode potential of platinum is forced positive, potentials may be reached to push the electrode potential into regions where platinum oxide is formed as well as platinum salts. Putting less charge in the secondary, anodic, phase forces the electrode less positive.

Why Biphasic Pulses and not Monophasic Pulses?

When a cathodic pulse is applied to an electrode, double-layer charging occurs along with any reduction reactions. At the termination of the current pulse, the electrode potential can decay by reactions driven by charge stored on the double layer (and pseudo capacitance), and in the case of electrodes in the living system, the reactions is oxygen reduction. Under resting conditions, the electrode potential of a platinum electrode can be found just positive where oxygen reduction occurs. The products of oxygen reductions are reactive oxygen species that, among other possibilities, react with nitrous oxide in the walls of blood vessels to induce vessel constriction and ischemia. Prolonged ischemia can lead to cell death. This reaction, occurring during the interpulse interval, can be eliminated by discharging the double layer (and pseudo capacitance) through a current pulse, anodic, supplied by the stimulator, thus a biphasic pulse. When Lilly [15] discovered biphasic pulses were less harmful than monophasic, he thought the harm was coming from displacement of the constituents of the cell wall and reasoned that a balance charge biphasic pulse would restore the displaced constituents. This is to origin of, what I call, the *dogma* in our field, *balanced charge biphasic pulses are the law*.

Adding a Delay Between the Cathodic Phase and the Anodic Phase of the Biphasic Pulse

In the preceding section, I have made the argument for biphasic stimulation. The first, usually cathodic, phase initiates the propagated action potential, and the second, anodic phase, is for the purpose of discharging the double layer (and pseudo capacitance) in order to terminate the electrochemistry driven by the cathodic phase. The down side to the second phase is that it can terminate/quench the development of the action potential [16]. This is because, when working with stimulus values slightly over threshold, the propagating action potential occurs after the termination of the cathodic phase. The quenching effect can be overcome by increasing the magnitude of the primary, cathodic, phase, but this violates the principal of minimizing charge injection. An alternative to increasing the cathodic charge injection is to add a delay between the primary and the secondary phases. The addition of the delay is illustrated in Fig. 3. The data presented were derived from an experiment where an intramuscular electrode was inserted into a muscle. The electrode was in the vicinity of the nerves innervating the muscle fibers, which means that some of the nerve fibers were closer to the electrode and some further from the current source, at the electrical threshold for excitation or slightly above threshold. In this experiment a monophasic pulse represents the control, dashed line. When the delay between the primary and the secondary pulse was zero, the evoked muscle response was ~45 % of the monophasic response. As the delay between the two phases was increased, the evoked muscle response increased. Most devices, that are capable of adding a delay, use a 100 μS delay between the two phases. The results shown were for nerves innervating muscles, but the results apply to virtually all neurostimulation devices.

The Neural Stimulating Community Needs to Have a Better Understanding of the Processes that Takes Place at the Electrode-Electrolyte Interface

A better understanding will enable us to determine which mechanisms are at play in tissue damage and electrode damage. This knowledge will enable us to engineer technology to safely

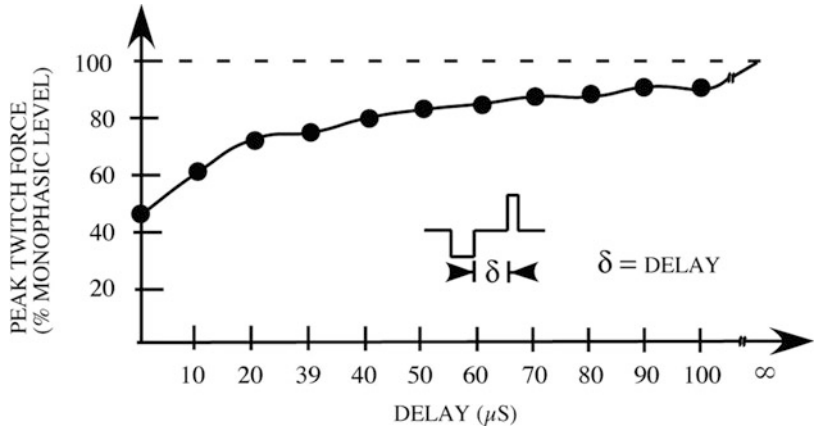

Neural Stimulation Electrodes and Sensors, Fig. 3 Evoked muscle force as a function of the delay between the primary, cathodic, and secondary, anodic, pulses of a biphasic stimulus. The *dashed line* represents the force recorded for a single cathodic stimulus pulse. The anodic phase is added to terminate the electrochemistry driven by charge accumulated on the double layer during the cathodic phase. If the anodic phase is applied immediately after the termination of the cathodic phase, the activation of nerve fibers not super maximally depolarized will be quenched, and no propagated action potential will occur. For most applications, a delay of 100 μS is deemed a reasonable period for the action potential to develop following a slightly depolarizing stimulus [16]

push more charge through the electrode than we now can. This knowledge may also be of use in litigation. At this time, too many neural stimulating devices must be operated at near the maximum safe limits before they begin to produce the desired result, be it a therapeutic effect or an evoked sensory percept, so a looming need is to find ways to inject more charge safely.

Future Directions

The neurostimulating community needs know the reactants that are generated during neural stimulation. If the reactions are known and the impact the reaction products have on cells in and around electrodes, life could be easier. For instance, workarounds could be reasoned rather than guessed, fewer animal experiments would be required, and litigation costs could be reduced. Too many devices in human use must use the maximum allowable stimulus to begin to attain the desired therapeutic effect; we need to be able to inject safely more charge than is currently possible. Further, it would be desirable to be able to do the job with batteries that are physically smaller than those currently used and preferable to not have to use larger batteries to get the job done. I can think of several ways to accomplish this increase:

1. Understand the charge transfer processes that **do** occur on the electrodes when current densities are applied in the range of neural stimulation applications.
2. Understand the charge transfer processes that occur on electrodes operating in living systems, lower order animals, and higher order animals and how these processes differ from studies in highly controlled electrolytes, e.g., sulfuric acid and phosphate buffered saline. As indicated in this document, narrow pulses are more charge efficient than are wider pulses. Therefore, studies must include pulses in the 10 μs to several hundred microsecond ranges.
3. Explore the imbalanced biphasic waveform, less anodic charge than cathodic, as a way to extend the excitation range.
4. Explore materials that will allow charge injections through reactions that are reversible within the time frame of the two phases of the stimulus pulse.

The cyclic voltammograms, when used in various electrolyte media, have been valuable tools to learn about potential reactions that **might** occur during neural stimulation in those media, but more information is needed to understand what actually occurs during the high current density, short pulse width, and conditions imposed during neural stimulation.

What is the potential range for the generation of corrosion products of platinum in different electrolytes? What are these products and do they interfere with cell function?

With stainless steel, we know that imbalanced biphasic stimulation of muscle cells is a safe way to avoid corrosion and more than triple charge injection limits imposed by balanced charge stimulation. There is no obvious reason to think imbalanced biphasic stimulation shouldn't be safe with electrodes in the brain, cells are cells, and it appears that the corrosion products are the culprits, which occur during the anodic phase. If a *reference electrode could be developed for implantable pulse generator*, IPG, closed-loop control could be used to eliminate electrode potentials that push the metal into regions where metal loss occurs.

The limits for the cathodic phase of an imbalanced biphasic pulse are not known because the mechanism for tissue injury is not known for this paradigm. The dogma in the neurostimulating community is that water reduction must be avoided; it surely was not with the imbalanced biphasic pulses that were safely applied to muscle.

Iridium oxide, belonging to a class of materials called super capacitors or variable valence materials, is an electrode material that has drawn considerable interest in the neural stimulating community [17] because the large pseudo capacitance, 100 times greater than that measured for platinum, based on slow cyclic voltammetry. The attractive feature of these materials is that the electron transfer processes are accommodated by valance changes within the oxide film, reversible reduction and oxidation between Ir^{+3} and Ir^{+4}, and movement of the counter ion in the hydrated oxide. This material, though used in research projects, is not yet used in commercially available devices. Though not a review article, Cogan [18] covers many of the findings for iridium oxide microelectrodes.

Concluding Remarks

The business end of a neural prosthetic device is the electrode, the metal-tissue interface, through which the device is to do a job, safely and efficiently. Understanding how these electrodes operate will provide insight into the mechanisms of tissue injury and ways to extend their charge injection capacities.

The most charge efficient way to activate neural tissues is to use the narrowest possible cathodic pulse followed by a delay of ~100 μS and then an anodic pulse. The function of the cathodic phase is to initiate a propagated action potential. The function of the delay phase is to avoid quenching the nascent action potential evoked in nerves driven to or slightly above threshold. The function of the anodic phase is to bring the interface potential back to the prepulse value. Bringing the electrode potential back to prepulse values (1) terminates reactions that can be driven by the potential across the electrode interface at the termination of the cathodic phase and (2) returns the interface potential to the prepulse value for the next succeeding stimulus pulse.

Tunable electrodes will be the way of the future. Using electrodes with multiple contacts through which electric fields in the tissue space can be shaped will enable purveyors of neural prostheses to electronically adjust or improve the efficacy without physically moving the electrode relative to the target tissue. These techniques, field steering, will likely utilize both anodic and cathodic first pulse paradigms.

The electrochemistry occurring on stimulating electrodes must be known much better than it is now. Cyclic voltammograms and classical ways of thinking of reactions do not tell the story for electrodes operating in the 1 A/cm^2 range for 100 μS. Porous surfaces may look good with slow cyclic voltammetry, but ions in the

electrolyte may not move fast enough to utilize the full surface area.

Finally, knowledge related to electrode operation must be digestible by engineers and scientist who are not trained or familiar with electrochemistry: the electrochemistry community must do a better job of communicating knowledge about how electrodes work in living systems.

Cross-References

- ▶ Electrode
- ▶ Neurons, Coupling
- ▶ Sensors

References

1. Grill WM, Kirsch RF (2000) Neuroprosthetic applications of electrical stimulation. Assist Technol 12(1):6–20
2. Shannon RV (1992) A model of safe levels for electrical stimulation. IEEE Trans BME 39(4):424–426
3. Cogan SF, Guzelian AA et al (2004) Over-pulsing degrades activated iridium oxide films used for intracortical neural stimulation. J Neurosci Methods 137(2):141–150
4. McCreery DB, Agnew WF et al (1990) Charge density and charge per phase as cofactors in neural injury induced by electrical stimulation. IEEE Trans Biomed Eng 37(10):996–1001
5. McCreery DB, Agnew WF et al (1988) Comparison of neural damage induced by electrical stimulation with faradaic and capacitor electrodes. Ann Biomed Eng 16(5):463–481
6. Mortimer JT, Kaufman D et al (1980) Intramuscular electrical stimulation: tissue damage. Ann Biomed Eng 8(3):235–244
7. Peterson DK, Nochomovitz ML et al (1994) Long-term intramuscular electrical activation of the phrenic nerve: safety and reliability. IEEE Trans Biomed Eng 41(12):1115–1126
8. Pudenz RH, Bullara LA et al (1975) Electrical stimulation of the brain III. The neural damage model. Surg Neurol 4(4):389–400
9. Robblee LS, McHardy J et al (1983) Electrical stimulation with Pt electrodes. VII. Dissolution of Pt electrodes during electrical stimulation of the cat cerebral cortex. J Neurosci Methods 9(4):301–308
10. Yuen TG, Agnew WF et al (1981) Histological evaluation of neural damage from electrical stimulation: considerations for the selection of parameters for clinical application. Neurosurgery 9(3):292–299
11. Scheiner A, Mortimer JT et al (1990) Imbalanced biphasic electrical stimulation: muscle tissue damage. Ann Biomed Eng 18(4):407–425
12. Rosenberg B, Vancamp L et al (1965) Inhibition of cell division in *Escherichia coli* by electrolysis products from a platinum electrode. Nature 205:698–699
13. Alderden RA, Hall MD et al (2006) The discovery and development of cisplatin. J Chem Educ 83(5):728–735
14. Agnew WF, Yuen TGH et al (1977) Neuropathological effects of intracerebral platinum salt injections. Neuropathol Exp Neurol XXXVI(3):533–546
15. Lilly JC, Hughes JR et al (1955) Brief noninjurious electrical waveform for stimulation of the brain. Science 121:468–469
16. van den Honert C, Mortimer JT (1979) The response of the myelinated nerve fiber to short duration biphasic stimulating currents. Ann Biomed Eng 7(2):117–125
17. Robblee LS, Lefko JL et al (1983) Activated Ir: an electrode suitable for reversible charge injection in saline. J Electrochem Soc 130:731–732
18. Cogan SF, Ehrlich J et al (2009) Sputtered iridium oxide films for neural stimulation electrodes. J Biomed Mater Res B Appl Biomater 89B(2):353–361

Neurons, Coupling

Andreas Offenhäusser
Institute of Complex Systems, Peter Grünberg Institute: Bioelectronics, Jülich, Germany

Introduction

Optimization of methodologies toward engineering the life sciences and healthcare remains a grand challenge. In the field of neurotechnology, tremendous progress has been made in a fundamental understanding of the nervous system and in building technology to diagnose and treat some neurological diseases. However, our understanding of nervous system function and technological approaches to measuring and manipulating neuronal circuits needs to be improved.

Neural prosthetic devices are artificial extensions of body parts which allow a disabled

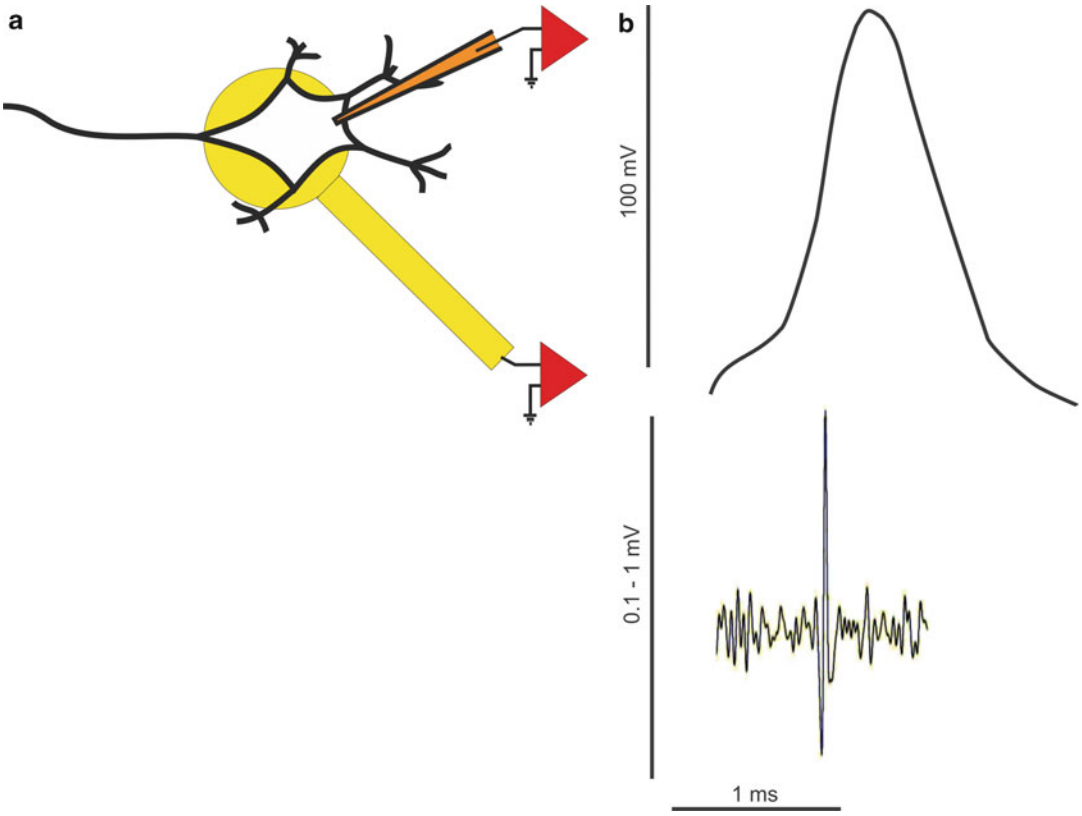

Neurons, Coupling, Fig. 1 (**a**) Schematic of a neuron on an extracellular electrode: intracellular (*upper orange* electrode) and extracellular (*lower yellow* electrode) signals can be recorded (**b**) Action potential of neuron (approx. 100 mV) recorded by an intracellular electrode (*upper trace*) and an extracellular electrode (*lower trace*)

individual to restore the body functions. Here, a neuroelectronic device which interfaces neuronal tissue with electronics is the key to restore the disabled body functions. Also, in vivo monitoring of the electrical signals from multiple cells during nerve excitation and cell-to-cell communication are important for design and development of novel materials and methods for laboratory analysis. In vitro biological applications such as drug screening and cell separation also require cell-based biosensors. Nowadays, the best approach to study the electrophysiological activity of neurons and cardiac cells in vitro and in vivo is based on planar microelectrode arrays or field-effect transistors which can be integrated with microfluidic devices. These methods allow the simultaneous monitoring and stimulation of large populations of excitable cells over many days and weeks and enable insights into long-term effects such as adaptivity in neuronal networks.

Basics

Silicon-based microstructures are gaining more and more importance in fundamental neuroscience and biomedical research. Precise and long-lasting neuroelectronic hybrid systems are in the center of research and development in this field. The interaction of a neuronal cell with an electronic device is schematically depicted in Fig.1a. Sufficient electrical coupling between the cell and the (gate) electrode for extracellular signal recording is achieved only when a cell or a part of a cell is located directly on top of the (gate) electrode. Electrical signals recorded by these devices show lower signals and a higher noise

level (owing to a weaker coupling to the (gate) electrode) compared to intracellular electrodes or patch pipettes (see Fig. 1b).

For extracellular signal recordings from electrically active cells in culture, two main concepts have been developed in the past: microelectrode arrays (MEAs) (see Fig. 2a) with metalized contacts on silicon or glass substrates have been used to monitor cardiac impulse propagation from dissociated embryonic myocytes [1–3], dissociated invertebrate neurons [4, 5] and mammalian neurons [6] spinal cord [7], and mouse dorsal root ganglia [8]. Alternatively, arrays of field-effect transistors (FETs) (see Fig. 2b) are used for extracellular recordings having either non-metalized transistor gates with cells growing directly on the gate oxide [9–11] or metalized gates. The latter were in direct contact with the electrolyte [12] or they were electrically insulated, so-called floating gates [13–15]. With these noninvasive methods, the electrical activity of single cells and networks of neurons can be observed over an extended period of time. Meanwhile both concepts are growing together

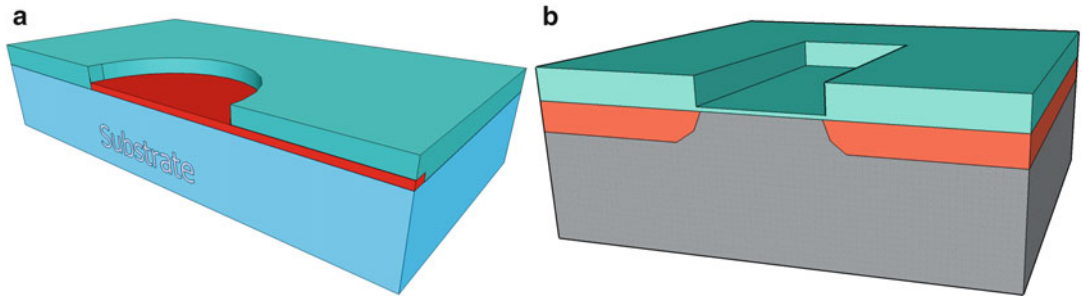

Neurons, Coupling, Fig. 2 (**a**) Substrate-embedded microelectrode: the metal electrode (*red*) is exposed to the electrolyte while the feed lines are covered with an isolation layer (*green-blue*) (**b**) Open-gate field-effect transistor for the recording of extracellular signals

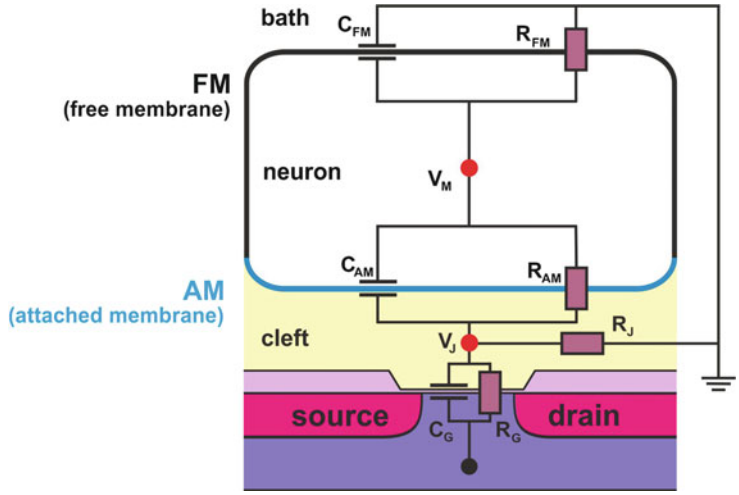

Neurons, Coupling, Fig. 3 Schematics of the neuroelectronic hybrid. The cell membrane is divided into free (*FM*) and attached membrane (*AM*) with the respective values of membrane area (A_{FM}, A_{JM}) and membrane capacitance (C_{FM}, C_{JM}) and resistance (R_{FM}, R_{JM}). C_G and R_G are the capacitance and the resistance of the (gate) electrode, respectively. The seal resistor R_J represents the electrical properties of the cleft between the membrane and the sensor surface. In case of patch-clamp experiments, the intracellular voltage V_M can be determined

by designing MEAs inside a CMOS process with on-chip amplification and filtering [16, 17].

Neuron-Electrode Coupling

For a quantitative understanding of the extracellular signals recorded by electronic devices, it is necessary to explain the experimental situation in detail. A schematic picture of a typical experimental situation is depicted in Fig. 3. Here, the neuroelectronic hybrid is formed by the neuron, the cleft between neuron and the sensor surface, and the electronic device. Outside the neuron and inside the cleft, there is extracellular electrolyte solution. By electrical excitation, the ion channels in the cell's membrane open and ions can flow from across the cell membrane. While in the upper part of the cell (free membrane), these ions just enter the surrounding electrolyte bath directly; it is different at the attached membrane. Here, the ions have to pass the cleft before entering/leaving the bath. The cleft acts as a resistance typically called seal resistance R_J [10, 18]. The magnitude of R_J is typically in the order of several 100 kW up to MW corresponding to a typical cleft thickness of 40–150 nm [19, 20]. The voltage V_J, which determines the voltage at the (gate) electrode, is mainly determined by the seal resistance R_J, and the current the flows across it.

Future Directions

Although this noninvasive method of extracellular recordings allows monitoring the electrical activity of single cells and networks of neurons over an extended period of time with good time resolution, it does not allow detecting subthreshold signals of neuronal cells. In the last years, a number of research groups began to study the combination of planar (2D) electrodes with intracellular recordings. This includes the use of gold mushroom-shaped protrusions, nanopillar electrodes, and nanorods. These developments may improve our understanding of neuroscience in the future [21–23].

Cross-References

▶ Neural Stimulation Electrodes and Sensors

References

1. Thomas CA, Springer PA, Loeb GE, Berwald-Netter Y, Okun LM (1972) A miniature microelectrode array to monitor the bioelectric activity of cultured cells. Exp Cell Res 74:61–66
2. Israel DA, Barry WH, Edell DJ, Mark RG (1984) An array of microelectrodes to stimulate and record from cardiac cells in culture. Am J Physiol 247: H669–H674
3. Connolly P, Clark P, Curtis ASG, Dow JAT, Wilkinson CDW (1990) An extracellular microelectrode array for monitoring electrogenic cells in culture. Biosens Bioelectron 5:223–234
4. Breckenridge LJ, Wilson RJA, Connolly P, Curtis ASG, Dow JAT, Blackshaw SE, Wilkinson CDW (1995) Advantages of using microfabricated extracellular electrodes for in vitro neuronal recording. J Neurosci Res 42:266–267
5. Regehr WG, Pine J, Rutledge DB (1989) A long-term in vitro silicon-based microelectrode–neuron connection. IEEE Trans Biomed Eng 35:1023–1031
6. Pine J (1980) Recording action-potentials from cultured neurons with extracellular micro-circuit electrodes. J Neurosci Methods 2:19–31. doi:10.1016/0165-0270(80)90042-4
7. Gross GW, Williams AN, Lucas JH (1982) Recording of spontaneous activity with photoetched microelectrode surfaces from spinal cord neurons in culture. J Neurosci Methods 5:13–22
8. Jimbo Y, Kawana A (1992) Electrical stimulation and recording from cultured neurons using a planar electrode array. Biochem Bioenerg 29:193–204
9. Bergveld P, Wiersma J, Meertens H (1976) Extracellular potential recordings by means of a field-effect transistor without gate metal, called OSFET. IEEE Trans Biomed Eng 23:136–144
10. Fromherz P, Offenhäusser A, Vetter T, Weis J (1991) A neuron-silicon junction: a Retzius cell of the leech on an insulated-gate field-effect transistor. Science 252:1290–1293
11. Offenhäusser A, Sprössler C, Matsuzawa M, Knoll W (1997) Field-effect transistor array for monitoring electrical activity from mammalian neurons in culture. Biosens Bioelectr 12:819–826
12. Jobling DT, Smith JG, Wheal HV (1981) Active microelectrode array to record from the mammalian central nervous-system in vitro. Med Biol Eng Comput 19:553–560
13. Offenhäusser A, Rühe J, Knoll W (1995) Neuronal cells cultured on modified microelectronic device surfaces (1995). J Vac Sci Tech A 13:2606–2612

14. Cohen A, Spira ME, Yitshaik S, Borghs G, Shwartzglass O, Shappir J (2004) Depletion type floating gate p-channel MOS transistor for recording action potentials generated by cultured neurons. Biosens Bioelectron 19:1703–1709
15. Meyburg S, Goryll M, Moers J, Ingebrandt S, Böcker-Meffert S, Lüth H, Offenhäusser A (2006) N-channel field-effect transistors with floating gates for extracellular recordings. Biosens Bioelectr 21:1037–1044
16. Heer F, Hafizovic S, Franks W, Blau A, Ziegler C, Hierlemann A (2006) CMOS microelectrode array for bidirectional interaction with neuronal networks. IEEE J Sol State Circ 41:1620–1629
17. Imfeld K, Neukom S, Maccione A, Bornat Y, Martinoia S, Farine P-A, Koudelka-Hep M, Berdondini L (2008) Large-scale high-resolution data acquisition system for extracellular recording of electrophysiological activity. IEEE Trans Biomed Eng 55:2064–2073
18. Rutten W (2002) Selective electrical interfaces with the nervous system. Ann Rev Biomed Eng 4:407–452
19. Lambacher A, Fromherz P (1996) Fluorescence interference-contrast microscopy on oxidized silicon using a monomolecular dye layer. Appl Phys A 63:207–216
20. Wrobel G, Höller M, Ingebrandt S, Dieluweit S, Sommerhage F, Bochem HP, Offenhäusser A (2007) Cell-transistor coupling: transmission electron microscopy study of the cell-sensor interface. J R Soc Interface 5:213–222
21. Hai A, Shappir J, Spira ME (2010) In-cell recordings by extracellular microelectrodes. Nat Methods 7:200–202
22. Almquist BD, Melosh NA (2010) Fusion of biomimetic stealth probes into lipid bilayer cores. Proc Natl Acad Sci USA 107:5815–5820
23. Brüggemann D et al (2011) Nanostructured gold microelectrodes for extracellular recording from electrogenic cells. Nanotechnology 22:265104

Ni-Cadmium Batteries

Takashi Eguro
Frukawa Battery, Iwaki, Fukushima, Japan

Introduction

A storage battery has supported a recent rapid expansion of the portable electronic device market and has been developed to the market where a further development has been expected such as eco-friendly cars market such as EV and HEV or the power supply market of an electricity accumulation system of a renewable energy such as sunlight and wind power. A nickel–cadmium secondary battery plays a role as a pioneer making the importance of the storage battery recognized in these fields and has been used in many fields still now.

The nickel–cadmium secondary battery was invented in 1899 by Waldemar Jungner as a durable storage battery which endures severe conditions of use such as overcharge/overdischarge/long-term leaving to which a lead-acid storage battery has been unsuitable and has been used for a long time in various fields with the lead–acid storage battery, until a nickel–hydrogen battery and a lithium ion battery appeared in 1990s.

History

The nickel–cadmium secondary battery was invented in 1899 by Waldemar Jungner, and was sometimes referred to as a "Jungner battery." The practically used "Jungner battery" is a vented type battery using pocket-type electrodes. Then, a sintered-type electrode which is excellent in high-rate discharge performance and low-temperature performance was invented, and the nickel–cadmium secondary battery has come to be used for many uses, such as aircraft starting, railroads, vehicles for industry, miner lamps, and emergency lighting.

Then, A. B. Lange and others found how a cadmium electrode consumes the oxygen from a positive electrode during overcharging in 1938. Then, G. Neumann and others established the present sealing principle and basic structure of a sealed-type nickel–cadmium secondary battery in 1948. Then, the sealed-type nickel–cadmium secondary battery has come to rapidly spread mainly in the consumer electronic equipment market.

In Japan, the Furukawa Battery Co., Ltd. industrialized a sintered-type vented nickel–cadmium battery for airplane starting in 1955. The Furukawa Battery Co., Ltd. started mass production of the vented-type nickel–cadmium secondary battery and a sealed nickel–cadmium secondary battery for industrial use in 1962 and developed the same to the fields, such as aircrafts,

railroads, backup power supply, and apparatus for emergency use.

On the other hand, Sanyo Electric Co., Ltd. started mass production of a consumer sealed type nickel–cadmium secondary battery. Then, other companies produced a consumer sealed-type nickel–cadmium secondary battery commercially one after another. Then, the batteries have been used as the main power supply of portable electronic devices such as cordless power tools and toys, video cameras, and notebook PCs in 1980s, and the production amount has enlarged drastically.

Although when a nickel–hydrogen battery and a lithium ion battery were produced commercially successively in 1990 and in 1991, respectively, the share of the portable electronic device market was taken by these batteries. However, the nickel–cadmium secondary battery is widely used currently in the fields, such as power tools, toys, aircrafts, railroads, backup power, and apparatus for emergency use.

Principle

The nickel–cadmium secondary battery contains NiOOH/nickel hydroxide as a positive active material, cadmium/cadmium hydroxide as a negative active material, and an aqueous solution containing potassium hydroxide as the main component as an electrolyte. Generally the charge-and-discharge reaction is shown in the following formulas 1, 2 and 3.

Positive active material:

$$NiOOH + H_2O + e^- \underset{\text{charge}}{\overset{\text{discharge}}{\rightleftharpoons}} Ni(OH)_2 + OH^- \qquad E_0 = +0.52\text{V} \tag{1}$$

Negative active material:

$$Cd + 2OH^- \underset{\text{charge}}{\overset{\text{discharge}}{\rightleftharpoons}} Cd(OH)_2 + 2e^- \qquad E_0 = -0.80\text{V} \tag{2}$$

Overall cell reaction

$$2NiOOH + Cd + 2H_2O \underset{\text{charge}}{\overset{\text{discharge}}{\rightleftharpoons}} 2Ni(OH)_2 + Cd(OH)_2 \tag{3}$$

Electromotive force: 1.32V

The actual reaction mechanisms are more complicated and are considered that the charge-and-discharge reaction at a positive active material is a reaction accompanied by the diffusion in the solid phase of a proton, and reaction at a negative active material is a dissolution/deposit reaction accompanied by an intermediate product.

Type

The electrodes of the nickel–cadmium secondary battery are classified into pocket type, sintered type, and pasted type according to those manufacturing methods. Moreover, the batteries are classified into vented-type cell and sealed-type cell according to the existence of sealing structure. The batteries are classified into a prismatic cell, a cylindrical cell, and a button cell according to shape.

Manufacturing Methods of Electrode

Pocket type
Sintered type
Pasted type
Cell type
Vented-type cell
Sealed-type cell

Shape
Prismatic cell
Cylindrical cell
Button cell

Pocket Type

The pocket-type electrode is the electrode structure used as the foundations of the "Jungner battery" and is characterized by filling up active materials into a "pocket" formed with perforated iron sheets. As for the manufacture method of a pocket-type cell is as follows.

The positive active material of a pocket-type electrode consists of nickel hydroxide powder by which cobalt hydroxide was coprecipitated, and is obtained from those mixed sulfate by a neutralizing method. Graphite powder is mixed as a conductor. The addition of cobalt is performed for increasing the capacity of the positive active material. Cadmium hydroxide which is a negative active material is manufactured by a coprecipitation method or a dry-mixing method. Moreover, iron powder is usually mixed with negative active material of a pocket type electrode for the increase in capacity. Graphite powder and/or nickel flake is mixed as a conductor.

These active material powders are molded by pressurizing to be formed into long and slender tabular briquettes. Then, these briquettes are wrapped in perforated iron sheets of a ribbon shape to form a pocket of a long and slender plate shape. A plate frame is welded to a substance obtained by engaging a plurality of the pockets to form a plate. There is a projecting lug in the upper part of the plate frame, and a large number of positive and negative electrodes are put together alternately, and then each pole is fixed with a bolt and a nut to the lugs of each pole plate group. There is no sheet-like separator between positive and negative electrodes, and pin-like resin is inserted between the positive and negative electrodes to prevent contact thereof. Thus, an element referred to as a pole plate group is completed. The electrode group activated in the formation process is inserted in a battery container, and the container is filled with an electrolyte. Usually, lithium hydroxide is added to an electrolyte for the increase in capacity. A prismatic container made of resin or iron is mainly used for the battery container. The usual pocket-type nickel–cadmium battery is a vented type and is provided with a lid having a vent for escaping gases generated from the electrode group during charge operation. This vent is provided also with the role for filling a cell with water or electrolyte.

The pocket electrodes have a strong structure and are excellent in durability and the manufacturing cost thereof is low, and therefore, the pocket electrodes have been used for miner lamps, railway vehicles, emergency backup power, etc. for a long time.

However, the pocket-type nickel–cadmium battery has low energy density and low output performance, requires frequent water supply, and is difficult to seal, and therefore the production amount thereof has decreased.

Sintered Type

The sintered-type electrode was developed in Germany in 1932. This electrode is characterized by filling up active materials by an impregnation method into a porous sintered plaque in which carbonyl nickel powder having an average particle diameter of several microns is sintered.

The production method of the porous sintered plaque includes a dry method and a wet method. With respect to the dry method, carbonyl nickel powder is spread to a Ni wire grid with a sieve or the like, adjusted to a predetermined thickness, and then sintered at 800–1,000° [Celsius] in a reducible gas atmospheres, such as hydrogen gas or butane reformed gas. With respect to the wet method, carbonyl nickel powder, a binder such as CMC or MC, and water are mixed to prepare a slurry. The slurry is applied to a nickel-plated iron thin sheet (perforated sheet) which has an open area ratio of about 50 %, and the thickness is adjusted in a scratching portion. Then, after drying with a drying furnace, it is sintered at a temperature of 800–1,000° [Celsius] in a reducible gas atmosphere. The typical porosity of the porous sintered plaque is 80–87 %.

The impregnation method is a method including impregnating the sintered plaque with a hot

impregnation liquid under normal pressure or decompression, neutralizing in a sodium hydroxide aqueous solution, and then filling up the inside of the porous sintered plaque with an active material. For a general impregnation liquid of a positive active material, an aqueous solution obtained by mixing nickel nitrate and a fixed quantity of cobalt nitrate is used. Then, a coprecipitated material of nickel hydroxide and cobalt hydroxide is obtained in a neutralization process. Usually, since a predetermined amount of an active material cannot be charged in one impregnation process, this process is repeated several times. This method is also referred to as a chemical impregnation method.

Moreover, there is a method referred to as an electrochemical impregnation method for depositing hydroxide in the plaque by carrying out the cathodic polarization of the plaque in the impregnation liquid. The electrochemical impregnation method has a merit such that an active material can be charged with a high density by a small number of times of impregnation. However, since the composition of the impregnation liquid changes with progress of electrochemical impregnation and by-products also tend to be formed, the method is used only for the limited use.

In the sintered electrode, a lug is formed at the end of the sheet to which the slurry is not applied or is attached by welding. Then, a large number of positive and negative electrodes are put together alternately inserting a separator. The pole is fixed to the lug with a bolt and a nut similarly as in the pocket type or is joined by resistance welding. Nylon or polypropylene cloth or nonwoven fabric is mainly used for a separator in the sintered-type nickel–cadmium secondary battery. Moreover, since the sintered-type plate is flexible compared with the pocket type, the sintered-type plate is able to be rolled in the shape of a bobbin combining positive electrodes, negative electrodes, and separators and can be stored in a cylindrical container. The cylindrical container is excellent in resistance to pressure and therefore is frequently used for the sealed-type nickel–cadmium secondary battery described later. The sintered-type electrode has high energy density, high-rate discharge characteristic, and high mass productionability by the wet sintering method. Therefore, currently, the sintered-type electrode is most widely produced in the nickel–cadmium secondary battery with the pasted-type electrode described later.

Pasted Type

The pasted-type electrode is developed in order to design a small and lightweight nickel–cadmium secondary battery. Main production methods of the pasted-type electrode include a method of applying to a nickel-coated steel sheet with perforations and a method of filling up a sponge-like nickel substrate.

The former is used for a cadmium negative electrode and the latter is mainly used for a nickel positive electrode.

A method for manufacturing a common pasted-type electrode for use in the cadmium negative electrode includes mixing a cadmium oxide activate material and PVA or the like with ethylene glycol to form a paste, applying the paste to a nickel-plated perforated iron sheet, and then drying the same to form a plate. The pasted-type electrode for use in the nickel positive electrode is obtained by filling up a slurry obtained by mixing a nickel hydroxide positive electrode active material, a binder, and water to a sponge-like nickel substrate having a relatively large pore diameter of 100 to several 100 μm, and then drying and pressing the same. There is also a method using a nickel substrate formed with nickel fiber in addition to the sponge-like nickel substrate. The assembly method of the electrode group is substantially similar to that of the sintered type.

Compared with the sintered-type electrode, the pasted-type electrode is able to achieve an increase in capacity of the electrode. Currently, the pasted-type electrode is used widely.

Vented Type Cell

In the completion or the end of charging, the storage battery containing an aqueous electrolyte causes electrolysis reaction of the water. Then oxygen generates from the positive electrode

and hydrogen generates from the negative electrode in accordance with the following formulas 4 and 5:

The oxygen generating reaction in positive electrode:

$$4OH^- \longrightarrow 2H_2O+O_2\uparrow+4e^- \quad (4)$$

The hydrogen generating reaction in negative electrode:

$$2H_2O+2e^- \longrightarrow H_2\uparrow+2OH^- \quad (5)$$

The oxygen recombination reaction in negative electrode:

$$2Cd+O_2+2H_2O \longrightarrow 2Cd(OH)_2 \quad (6)$$

$$O_2+2H_2O+4e^- \longrightarrow 4OH^- \quad (7)$$

Thus, it is necessary to have a vent valve for releasing the gas. Moreover, since alkaline mist splashes from the electrolyte in the battery with gas venting, the vent valve has a splash proof structure which prevents diffusion of mist. The nickel–cadmium secondary battery with such a structure is referred to as the vented-type cell.

The vented-type battery needs to perform "water addition" in which water consumed by electrolysis is periodically added. However, in recent years, the vented-type nickel–cadmium secondary battery which has reduced the "water addition" frequency is produced commercially for trains and the like. The battery controls the electrolysis of the water under float charging by using the pasted-type cadmium electrode which has a high hydrogen overpotential characteristic for the negative electrode.

A nickel–cadmium secondary battery with the type of the gas recombination by catalyst in which oxygen and hydrogen gas generated in the end of charging are made to react and return to water by providing a catalyst to the vent valve is used partly.

The capacity range of the vented-type cell is broad from several Ah(s) to hundreds Ah(s), and a comparatively large cell occupies the mainstream. The shape of the vented-type cell is only prismatic.

There is also a mono-block-type battery using mono-block container with some independent cell rooms divided with partitions.

Sealed-Type Cell

A.B. Lange and others discover and G. Neumann and others established the sealed battery principles of the gas recombination on the negative electrode are as follows in general.

It is configured so that oxygen gas is previously generated from the positive electrode in the end of charging by adjusting the negative electrode capacity to an excessive degree rather than the positive electrode capacity (referred to as "charge reserve").

Oxygen generated from the positive electrode is easily diffused to the negative electrode by limiting the amount of the electrolyte and by using a separator with high gas permeability.

Thus, it is necessary to have a vent valve for releasing the gas. Moreover, since alkaline mist splashes from the electrolyte in the battery with gas venting, the vent valve has a splash proof structure which prevents diffusion of mist. The nickel–cadmium secondary battery with such a structure is referred to as the vented-type cell.

The vented-type battery needs to perform "water addition" in which water consumed by electrolysis is periodically added. However, in recent years, the vented-type nickel–cadmium secondary battery which has reduced the "water addition" frequency is produced commercially for trains and the like. The battery controls the electrolysis of the water under float charging by using the pasted-type cadmium electrode which has a high hydrogen overpotential characteristic for the negative electrode.

A nickel–cadmium secondary battery with the type of the gas recombination by catalyst in which oxygen and hydrogen gas generated in the end of charging are made to react and return to water by providing a catalyst to the vent valve is used partly.

The capacity range of the vented-type cell is broad from several Ah(s) to hundreds Ah(s), and a comparatively large cell occupies the mainstream. The shape of the vented-type cell is only prismatic.

There is also a mono-block-type battery using mono-block container with some independent cell rooms divided with partitions.

An oxygen gas recombination reaction occurs on the negative electrode.

This oxygen gas recombination reaction is considered that two kinds of reactions occur as follows.

Since the charging of the negative electrode is limited in both the cases, the negative electrode does not result in a full charge state, so that hydrogen gas does not generate. Moreover, since the charge–discharge performance of the negative electrode is inferior to that of the positive electrode, a part of the negative electrode is beforehand charged (referred to as "pre-charge"). By performing "charge reserve" and "pre-charge," the charge-and-discharge process of the sealed-type cell is always regulated by the positive capacity. The capacity range of the sealed type battery is from several mAh(s) to tens Ah(s), and a small cell occupies the mainstream. The sealed-type cell has high flexibility of shape, such as a square cell, a cylindrical cell, and a button cell.

This sealed-type nickel–cadmium secondary battery is easy to downsize, is excellent in discharging characteristic, and requires no maintenance at all. Therefore, the sealed-type nickel–cadmium secondary battery has spread as the main power supply of portable electronic devices, such as cordless power tools, toys, video cameras, and notebook PCs, and has supported the development thereof.

Future Directions

Although the market of the nickel–cadmium battery is decreasing gradually with a rapid development of a lithium ion battery in recent years, the nickel–cadmium battery is still used due to high reliability and achievements thereof for many uses. Moreover, the history of the nickel–cadmium battery is also the history of the development of a high-performance electrode. Various knowledge that many ancient people had is kept alive for a development of a next-generation high-performance battery.

Cross-References

▶ Ni-Metal Hydride Batteries

References

1. Uno Falk S, Salkind AJ (1969) Alkaline storage batteries. Wiley, New York
2. Kubokawa S, Ikari S, Ikeda K, Tagawa H, Shimizu K, Takagaki T, Takahashi H, Takehara Z (1975) Denchi handbook (Ed. Z. Takehara). Denki-syoin, Tokyo, Chap. 3. [in Japanese]
3. Awajitani T, Kaiya H (2001) Denchi Binran (Ed. Y. Matsuda, Z. Takehara). Maruzen, Tokyo, Chap. 3.4. [in Japanese]

Ni-Metal Hydride Batteries

Munehisa Ikoma
Panasonic, Moriguchi, Japan

Introduction

Nickel/metal hydride (Ni/MH) battery is a secondary battery using hydrogen storage alloy for the negative electrode, $Ni(OH)_2$ for the positive electrode, and alkaline solution for the electrolyte. Polypropylene nonwoven fabric is usually selected for the separator. The theoretical voltage is about 1.32 V, and the operating voltage is about 1.2 V which is almost the same as that of Ni/Cd battery [1]. The Ni/MH battery has been put to practical use for portable electric equipments in 1990 and for HEV (hybrid electric vehicle) in 1997 [2, 3].

Reaction Mechanism

The electrode reaction and battery reaction are shown in formulas (1), (2), and (3),
at the positive electrode

$$NiOOH + H_2O + e^- \rightleftarrows Ni(OH)_2 + OH^- \quad (1)$$

at the negative electrode

$$MH + OH^- \rightleftarrows M + H_2O + e^- \quad (2)$$

total battery reaction

$$MH + NiOOH \rightleftarrows M + Ni(OH)_2 \quad (3)$$

M: hydrogen storage alloy

The reaction at the positive electrode is the same as that in Ni/Cd battery. At the negative electrode, hydrogen is absorbed in the alloy during the charge reaction, and the absorbed hydrogen is released and electrochemically consumed on the surface of the alloy during discharge. The battery reaction is relatively simple in that it basically involves hydrogen transportation between the positive and negative electrode.

During overcharge, oxygen is generated at the positive electrode as expressed formula (4). When the capacity of the negative electrode is sufficiently high, oxygen is absorbed by the negative electrode as shown in formula (5). This absorption reaction falls into equilibrium with the charging reaction as shown in formula (6), and so the state of charge of the negative electrode is kept:
at the positive electrode

$$OH^- \rightarrow 1/4O_2 + 1/2H_2O + e^- \quad (4)$$

at the negative electrode

$$MH + 1/4O_2 \rightarrow M + 1/2H_2O \quad (5)$$

$$M + H_2O + e^- \rightarrow MH + OH^- \quad (6)$$

Components

Positive Electrode

The sintered type and the pasted type are in popular in a positive electrode.

The sintered-type electrode is formed by filling of the nickel hydroxide active material into the sintered nickel porous layer on the punched steel metal. The pasted-type electrode is formed by filling of the nickel hydroxide active material into the formed nickel substrate with very high porosity. In the sintering layer of the sintered-type electrode, the pore size is around 10 μm and the porosity is approximately 75 %. On the contrary, in the formed nickel substrate of the pasted-type electrode, the pore size is around 500 μm and the porosity is approximately 95 %. Therefore, the sintered-type electrode is suitable for a high power use, and the pasted-type electrode is used for a high capacity battery [4].

Nickel hydroxide active material is provided by reacting nickel sulfate solution and an alkaline solution. A part of nickel of nickel hydroxide is substituted for Zn and Co for the improvement of the battery performance. The theory capacity of nickel hydroxide is 289 mAh/g by supposing one electron reaction. The utilization of nickel hydroxide of a sintered-type electrode is approximately 100 %, but that of a pasted-type electrode without a conductive additive is around 65 %. The improvement of the utilization is enabled by forming CoOOH conductive networks between nickel hydroxide particles. The cobalt compound (Co, CoO, $Co(OH)_2$) is filled into the formed nickel substrate with nickel hydroxide as an additive. The Co compounds form a conductive network as CoOOH by charging. To improve the conductivity of the cobalt conductive layer, $Co(OH)_2$ layer coating to the surface of nickel hydroxide particles and the oxidation treatment in an alkaline solution of this coated powder are suggested.

Negative Electrode

In the Ni/MH battery, hydrogen storage alloy, which contains no poison and is environment friendly compared with conventional Ni/Cd battery, is utilized as the negative electrode.

The negative electrode is obtained by coating the hydrogen storage alloy paste on the punched steel metal. The paste consists of the mixture of the hydrogen storage alloy powder, the conductive additives, and the binder.

Hydrogen storage alloy is able to store more than 1,000 times quantity of hydrogen compared with the liquid hydrogen. For application of hydrogen storage alloy to Ni/MH battery, the following conditions are required:

1. Electrochemically reversible absorption and desorption of hydrogen in large quantities
2. Minimal deterioration during repeated hydrogen absorption and desorption (superior in oxidation resistance)
3. Chemical stability over a wide humidity range
4. Easy to handle and of high safety
5. High environmental conformity
6. Abundance of resources and relatively inexpensive.

AB type (TiFe), AB_2 type ($ZrMn_2$,ZrV_2,$ZrNi_2$), AB_5-type ($CaNi_5$,$LaNi_5$,$MmNi_5$), A_2B type (Mg_2Ni,Mg_2Cu), bcc type (V based), and superlattice type (mixture of AB_5 type and AB_2 type) have been studied, but with consideration of the abovementioned condition (1), (2), (3), (4), (5), and (6), only the AB_5-type alloy and the superlattice-type alloy have been put to practical use.

The alloy composition suitable for a negative electrode with high capacity is selected from the pressure-composition isotherms (PCT curves) which are obtained from the absorption and desorption reactions of the alloy with hydrogen. The AB_5-type alloys which are most often adopted for battery consist of $LaNi_5$ or $MmNi_5$ in which La is displaced by inexpensive Mm (mischmetal, a mixture of rare earth elements). $MmNi_5$ alloy is promising for the low costs, but with a high hydrogen equilibrium pressure, charging and discharging are difficult under room temperature and nominal pressure. For achieving a high capacity alloy, substituting a part of Ni in a $MmNi_5$ alloy with other metal elements is attempted. In addition, thermal treatment is applied for homogenizing composition and enhancing crystallinity to flatten the plateau part of the PCT curve, thereby achieving a high capacity.

The cycle life of the Ni/MH battery strongly depends on the characteristics of the negative electrode. Hydrogen storage alloy is pulverized and corroded during charge–discharge cycles in an alkaline solution. The pulverization properties of alloy can be controlled by substitution a part of Ni with Co [5]. In the Ni/MH battery with AB_5-type alloy, there is the problem of the long-term storage performance caused by the dissolution of Co and/or Mn which are the constituent element of the alloy. This problem is solved by adopting the rare earth–Mg–Ni type superlattice alloy which does not include Co and Mn in a constituent element. This alloy has a structure that AB_5-type structure and AB_2-type structure arranged regularly [6].

Separator

The nonwoven polyolefin fabric is used. The thickness of the separator is 100–200 μm, and the basis weight of the fiber is 50–80 g/m^2. The hydrophilicity is provided to the fiber surface of the separator with the sulfonation treatment, plasma treatment or acrylic acid graft polymerization treatment.

Application

The Ni/MH battery has been put to practical use for the power supply for the camcorder and the cellular phone in 1990.

After practical use, the energy density of the battery is doubled from 180 to 350 Wh/L by the development of the various technologies such as active material composition, surface treatment, and additives. This battery has been put to practical use for the power supply for the power tool by the improvement of the high output performance. The AA size and AAA size batteries that are compatible with a dry cell have been also put to practical use. This battery system has been put to practical use for HEV (hybrid electric vehicle) by the establishment of the battery management technology

and the improvement of the battery performance (the input/output performance and the durability) in 1997.

Future Directions

The energy density of the Ni/MH battery is smaller than that of the Lithium ion battery. But the Ni/MH battery is superior in the general performance balance such as input power density, output power density, cycle life, safety, reliability, recyclability, the cost. This superior general performance balance will bring up the market of the Ni/MH battery as the power supply for HEV and compatible with a dry cell in future.

The improvement of the hydrogen storage alloy is important to the performance enhancement of the Ni/MH battery. The detailed analysis and improvement of the chemical formula, structure and surface state of the hydrogen storage alloy shall lead the Ni/MH battery to the performance enhancement. In addition, the surface treatment technology, the other device and the battery management technology should be improved for the maximization of the battery performance.

Cross-References

► Ni-Cadmium Batteries

References

1. Ogawa H et al (1989) Proceedings of the 16th international power sources symposium, Bournemouth, pp. 393–410
2. Yuasa K et al (1991) Cylindrical type sealed nickel-metal hydride battery. Natl Tech Rep 37(1):44–51
3. Morishita N et al (1998) Nickel-Metal Hydride Battery for EV and HEV. Matsushita Tech J 44(4):426–433
4. Kaiya H et al (1986) New type high capacity nickel-cadmium battery (SM30). Natl Tech Rep 32(5):631–638
5. Ikoma M et al (1999) Effect of alkali-treatment of hydrogen storage alloy on the degradation of Ni/MH batteries. J Alloy Compd 284:92
6. Ochi M et al (2012) Nickel-metal hydride battery for hybrid electric vehicles (HEVs). Panasonic Tech J 57(4):278–283

Nickel Oxide Electrodes

Masanobu Chiku
Department of Applied Cemistry,
Graduate School of Engineering,
Osaka Prefecture University, Osaka, Japan

Introduction

A wide variety of metal oxides are investigated as electrode materials for electrochemical capacitors (super capacitors, ultracapacitors). Ruthenium oxide and iridium oxide are frequently used due to its high charging-discharging capacities. However, ruthenium and iridium are high cost and limited resources on the earth. Thus wide varieties of transition metals are studied as the electrode materials to alternate precious metals. Nickel oxide is one of the promising materials for high-performance electrode materials for electrochemical capacitors due to its low cost, high reservation on the earth, and low toxicity for environment.

Mechanisms

Nickel hydroxide exists in four different forms: α-$Ni(OH)_2$, β-$Ni(OH)_2$, β-NiOOH, and γ-NiOOH. β-$Ni(OH)_2$ and β-NiOOH are known as stable forms. The electrochemical reaction of NiO, $Ni(OH)_2$, and NiOOH is described as below:

$$Ni(OH)_2 + OH^- \leftrightarrow NiOOH + H_2O + e^- \quad (1)$$

$$NiO + OH^- \leftrightarrow NiOOH + e^- \quad (2)$$

Preparation of Nickel Oxide Electrodes

To prepare nickel oxide electrodes, nickel hydroxide precursors are frequently used, and nickel hydroxides are thermally oxidized to nickel oxide (Fig. 1). Industrially produced nickel hydroxide active materials are mainly used as

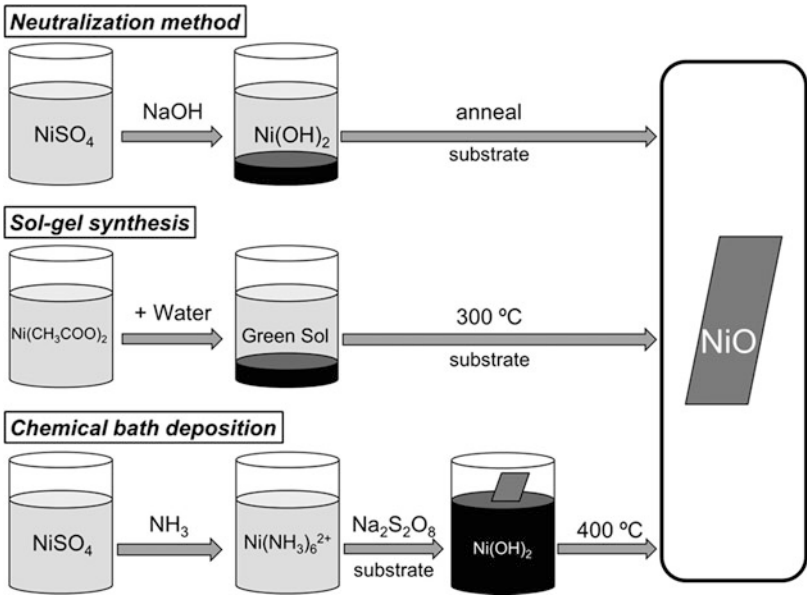

Nickel Oxide Electrodes, Fig. 1 Schematic images of the NiO electrode preparation

positive electrode for nickel-metal hydride secondary battery, and they are produced by using coprecipitation methods. Neutralization method is one of the most basic coprecipitation methods to prepare nickel hydroxide. The general neutralization method is described as follow: putting nickel sulfate solution by drops into alkali solution such as NaOH solution to neutralize and precipitate nickel hydroxide. After dried nickel hydroxide, it was washed with hot water to remove nickel sulfate and dried less than 150 °C to obtain nickel hydroxide powder.

Liu et al. applied sol–gel method to prepare nickel oxide active materials for electrochemical capacitors [1]. They dried nickel acetate tetrahydrate at 100 °C and stirred it in water for 2 days. The precipitants were separated by centrifugation and put it into water to get pale-green sol. Dipping coated the sol on nickel sheets and annealed in air at 300 °C for 1 h. The diameters of resultant nickel oxide were 3 ∼ 8 nm and pore sizes were 2 ∼ 3 nm. The electrochemical capacitors using resultant nickel oxide indicated 50 ∼ 64 F g^{-1} capacitance with 1 M KOH aqueous solution.

Inoue et al. applied chemical bath deposition (CBD) method to prepare nickel oxide electrodes [2].

Ammonia water was put into nickel sulfate aqueous solution at 30 °C. Then potassium persulfate aqueous solution was added into the solution, followed by stirring for 3 min. The resultant solution is named a CBD bath. A Ni foam as a substrate was soaked in CBD bath. Then the nickel hydroxide was deposited on Ni foam and annealed in air at 400 °C. The diameter of resultant nickel oxide particle was ca. 5 μm and flowerlike form. The electrochemical capacitors using resultant nickel oxide indicated ca. 80 F g^{-1} capacitance with 10 M KOH aqueous solution.

Future Perspective

Several types of NiO or $Ni(OH)_2$ electrode such as flowerlike [3], mesoporous [4], nanotubes [5], and nanorod [6] were investigated as active materials for electrochemical capacitors. These Ni oxide electrodes are combined with carbon negative electrodes to construct the hybrid capacitors with high capacity and power density [2]. However, there still remaining serious problems with life cycle, reducibility, long-term stability, etc. It would need some more innovation for the practical use of these high-performance electrode materials.

Cross-References

- ▶ Electrode
- ▶ Super Capacitors

References

1. Liu KC, Anderson MA (1996) Porous nickel oxide/nickel films for electrochemical capacitors. J Electrochem Soc 143:124–130
2. Inoue H, Namba Y, Higuchi E (2010) Preparation and characterization of Ni-based positive electrodes for use in aqueous electrochemical capacitors. J Power Sources 195:6239–6244
3. Xu LP, Ding YS, Chen CH, Zhao LL, Rimkus C, Joesten R, Suib SL (2008) 3D flowerlike α-nickel hydroxide with enhanced electrochemical activity synthesized by microwave-assisted hydrothermal method. Chem Mater 20:308–316
4. Xing W, Li F, Yan ZF, Lu GQ (2004) Synthesis and electrochemical properties of mesoporous nickel oxide. J Power Sources 134:324–330
5. Kim JH, Zhu K, Yan Y, Perkins CL, Frank AJ (2010) Microstructure and pseudocapacitive properties of electrodes constructed of oriented nio-tio2 nanotube arrays. Nano Lett 10:4099–4104
6. Hasan M, Jamal M, Razeeb KM (2012) Coaxial NiO/Ni nanowire arrays for high performance pseudocapacitor applications. Electrochim Acta 60:193–200

Nitrogen Oxides (NOx) Removal

Jorge G. Ibanez[1] and Krishnan Rajeshwar[2]
[1]Department of Chemical Engineering and Sciences, Universidad Iberoamericana, México, Mexico
[2]The University of Texas at Arlington, Arlington, TX, USA

Introduction

Nitrogen oxides in the atmosphere participate in environmentally challenging processes such as the greenhouse effect, acid rain, and photochemical smog. Their chemical reduction involves the use of a reducing agent whose storage and leakage (or *slip*) may be problematic [1]. A plausible alternative involves their electrochemical treatment, although this necessitates that the gases be dissolved in aqueous solution, which may not be a straightforward task. In addition, complex chemical equilibria exist among the different nitrogen oxides (see Fig. 1), derived in part from the varied oxidation states of nitrogen (i.e., from −3 to +5) [2–4].

Specific aspects of their electrochemistry and electrochemical reduction aimed at their removal are discussed next.

Nitrogen (I) Oxide

Also called nitrous oxide, dinitrogen monoxide, sweet air or laughing gas, N_2O is the most stable nitrogen oxide which – coupled with its IR absorption properties – makes its participation inevitable in the greenhouse effect. It can be electroreduced in alkaline and acidic media. Current efficiencies up to 100 % have been reported. Pd and macrocyclic amine complexes catalyze this electroreduction to $N_{2(g)}$ [2, 5]. The presence of N_2O can be used to advantage by forming an N_2O–H_2 fuel cell [5].

Nitrogen (II) Oxide

Also called nitric oxide, nitrogen monoxide or oxidonitrogen, NO is a colorless, relatively unreactive radical that is essentially insoluble in aqueous solution. Simple absorption in alkaline solutions is not effective, since it is only physically absorbed [3, 4, 6]. Absorption in nitric acid decreases with acid concentration [4], and oxidation with ozone to produce acidic NO_2 facilitates its absorption in alkaline media [6]. Absorption of NO with simultaneous oxidation at a gas diffusion electrode in alkaline solution eliminates the need for an oxidizing agent [6]:

$$NO + OH^- = NO_2^- + H^+ + e^- \qquad (1)$$

Aqueous absorption of NO is also facilitated by aminopolycarboxylate chelates of Fe(II) and Co(II) [7–10]. The resulting compounds can

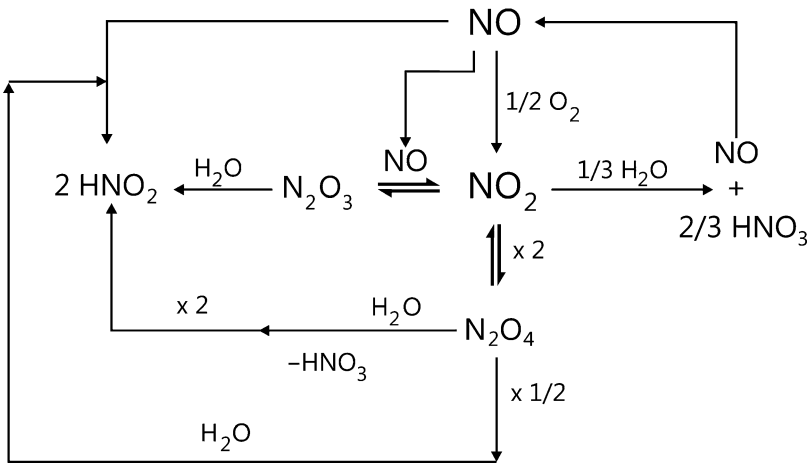

Nitrogen Oxides (NOx) Removal, Fig. 1 Nitrogen oxides chemical equilibria (Adapted from [2])

then be chemically or electrochemically reduced to yield hydroxylamine, hydrazine or ammonia, regenerating the chelate. Removal of NO from flue gases is facilitated by its preferential adsorption on noble metal catalysts. This allows for its reduction to occur at high yields even in dilute gas streams and in the presence of other competitive species (e.g., O_2, SO_2) [11]. In addition, by adjusting the electrode potential to place the valence electrons of the electrode at an energy level between that of the antibonding orbitals of NO and O_2, the competitive O_2 reduction can be inhibited [1]. Although electronically similar to CO, NO has an unpaired electron and a $2\pi^*$ orbital of lower energy that make it substantially more reactive towards oxidation and reduction [12].

The reduction of NO to produce ammonia, N_2O and hydroxylamine is thermodynamically allowed (see Table 1) and electrochemically viable [13, 14]. On this basis, an electrogenerative process has been proposed whereby NO reacts in a cell with protons and electrons at one electrode and H_2 at the other electrode to generate current [11]. Note that this configuration resembles that of a fuel cell (although the reactions are not necessarily the same), and the corresponding technology can be borrowed from that field. Electrogenerative processes can be defined as those in which favorable thermodynamic and kinetic factors are utilized for the production of coupled electrode reactions that take place in separate compartments in an electrochemical cell with simultaneous generation of electricity [11, 15–19].

Nitrogen Oxides (NOx) Removal, Table 1 Reduction of NO to environmentally friendlier products [2]

$2NO + 2H^+ + 2e^- \rightarrow N_2O + H_2O$
$2NO + 4H^+ + 4e^- \rightarrow N_2 + 2H_2O$
$2NO + 6H^+ + 6e^- \rightarrow 2NH_2OH$
$2NO + 10H^+ + 10e^- \rightarrow 2NH_3 + 2H_2O$

Nitrogen (IV) Oxide

Also called nitrogen dioxide or dioxidonitrogen, NO_2 is a brownish acidic radical whose electrochemistry follows essentially that of NO, as they have a common electroactive precursor, namely NO^+ [20].

Complex Nitrogen Oxides

The complex nitrogen oxides N_2O_4 and N_2O_3 undergo chemical absorption in aqueous solutions more easily than NO and NO_2, forming nitrogenated species susceptible to reduction [3].

Other General Treatments for NO_x

The electroreduction of NO_x in industrial waste gas streams can simultaneously lead to useful

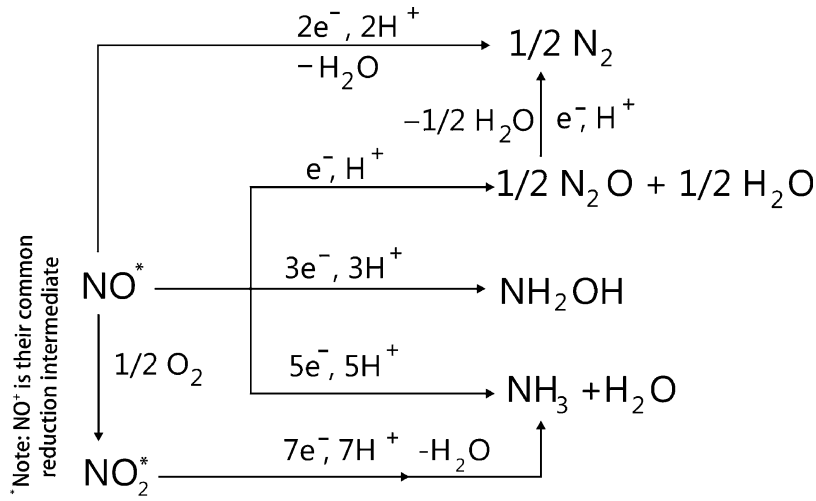

Nitrogen Oxides (NOx) Removal, Fig. 2 NOx reduction (Adapted from [2])

and/or inert compounds, as shown in Fig. 2 [8, 11, 15–18, 21, 22]. A major fraction of the current at low potentials may result in formation of ammonia and hydroxylamine [15–17]. Ammonia formation is strongly favored in N_2 diluent alone, whereas a trend towards hydroxylamine formation has been observed in the presence of CO or SO_2 [15–17]. A simultaneous desulfurization/denoxing process (called the Saarberg-Hölter-Lurgi, SHL process) is based on this principle [7]. Mixed ionic-electronic conducting catalytic membranes allow the reduction of NO_x by acting as short circuited devices, where the electrons reduce the oxides while the oxide ions thus produced move towards a low pressure end, completing the process [1, 2]. The catalytic activity and selectivity of porous metal films deposited on solid electrolytes for the reduction of NO_x with H_2 or CO can be substantially promoted by the application of an external potential or current [14, 23, 24]. This non-faradaic electrochemical modification of catalytic activity (NEMCA) is envisaged as a plausible technology in the near future [25].

Future Directions

Optimization of the conductivity of solid oxide ion conducting electrolytes is essential to lower the temperatures required for the reduction of NO_x [1]. In addition, the development of more selective layers can potentially increase the efficiency of electroreduction devices by avoiding the undesired reduction of O_2 [26–28].

References

1. Kammer Hansen K (2000) Electrochemical reduction of NO and O_2 on Cu/CuO. J Appl Electrochem 30:193–200
2. Rajeshwar K, Ibanez JG (1997) Environmental electrochemistry: fundamentals and applications in pollution abatement. Academic, San Diego
3. Weisweiler W, Deib K-H (1987) Influence of electrolytes on the absorption of nitrogen oxide components N_2O_4 and N_2O_3 in aqueous absorbents. Chem Eng Technol 10:131
4. Weisweiler W, Eidam K, Thiemann M, Scheibler E, Wiegand KW (1991) Absorption of nitric oxide in dilute nitric acid. Chem Eng Technol 14:270
5. Tomkiewics M, Yoneyama H, Haynes R, Hori Y (eds) (1993) Environmental aspects of electrochemistry and photoelectrochemistry, vol 93-18, The Electrochemical Society, proc. The Electrochemical Society, Pennington
6. Furuya N, Okada T (1991) Electrooxidation of NO on gas-diffusion electrode. In: 179th meeting of the Electrochemical Society, Washington, DC, 5–10 May 1991. Extended Abstract # 728
7. van Velzen D (1992) Electrochemical processes in the protection of the environment. In: Genders D, Weinberg N (eds) Electrochemistry for a cleaner environment. The Electrosynthesis Co. East Amherst, New York
8. Uchiyama S, Muto G (1981) Dependence of pH and chelate ligand on the electroreduction mechanism of

a nitrosyl-aminopolycarbonato-ferrous complex in weakly acidic media. J Electroanal Chem 127:275
9. Long X-L, Xiao W-D, Yuan W-K (2005) Kinetics of gas–liquid reaction between NO and $Co(en)_3^{3+}$. Ind Eng Chem Res 44:4200–4205
10. Ibanez JG, Hernandez-Esparza M, Doria-Serrano C, Fregoso-Infante A, Singh MM (2008) Environmental chemistry: microscale laboratory experiments. Springer, New York
11. Pate KT, Langer SH (1985) Electrogenerative reduction of nitric acid for pollution abatement. Environ Sci Technol 19:371–373
12. de Vooys ACA (2004) Mechanisms of electrochemical reduction and oxidation of nitric oxide. Electrochim Acta 49:1307–1314
13. de Vooys ACA (2001) Mechanistic study of the nitric oxide reduction on a polycrystalline platinum electrode. Electrochim Acta 46:923–930
14. Petrushina IM (2003) Electrochemical promotion of NO reduction by hydrogen on a platinum/polybenzimidazole catalyst. J Electrochem Soc 150: D87–D90
15. Langer SH, Foral MJ, Colucci JA, Pate KT (1986) Electrogeneration and related electrochemical methods for NO_x and SO_x control. Environ Prog 5:277
16. Foral MJ, Langer SH (1988) The effect of preadsorbed sulfur on nitric oxide reduction at porous platinum black electrodes. Electrochim Acta 33:257
17. Foral MJ, Langer SH (1991) Sulfur coverage effects on the reduction of dilute nitric oxide at platinum black gas diffusion electrodes. Electrochim Acta 36:299
18. Langer S (1994) Electrochemical processing without a power source: benefits and applications. In: Eighth international forum on electrol in the chemical industries. The Electrosynthesis Co., Orlando
19. Yap CY, Mohamed N (2008) Electrogenerative processes for environmental applications. Clean 36:443–452
20. Snider BG (1979) Reduction of nitric oxide, nitrous acid and nitrogen dioxide at platinum electrodes in acidic solutions: review and new voltammetric results. Anal Chim Acta 105:9–23
21. Langer SH, Pate KT (1980) Electrogenerative reduction of nitric oxide. Nature 284:434
22. Furuya N, Murase K (1994) Electroreduction of nitric oxide to nitrogen using a gas diffusion electrode loaded with noble metals. In: 186th meeting of the Electrochemical Society, Miami Beach, Abstract # 589
23. Pliangos C (2000) Electrochemical promotion of a classically promoted Rh catalyst for the reduction of NO. Electrochim Acta 46:331–339
24. Dorado F, de Lucas-Consuegra A, Vernoux P, Valverde JL (2007) Electrochemical promotion of platinum impregnated catalyst for the selective catalytic reduction of NO by propene in presence of oxygen. Appl Catal B Environ 73:42–50
25. Vernoux P, Gaillard F, Lopez C, Siebert E (2003) Coupling catalysis to electrochemistry: a solution to selective reduction of nitrogen oxides in lean-burn engine exhausts? J Catal 217:203–208
26. Hamamoto K (2006) Intermediate temperature electrochemical reactor for NO_x decomposition. J Electrochem Soc 153:D167–D170
27. Wang X (2004) Selective decomposition of NO in the presence of excess O_2 in electrochemical cells. J Appl Electrochem 34:945–952
28. Kammer K (2005) Electrochemical deNO_x in solid electrolyte cells—an overview. Appl Catal B Environ 58:33–39

Non-Aqueous Electrolyte Solutions

Heiner Jakob Gores[1] and Hans-Georg Schweiger[2]
[1]Institute of Physical Chemistry, Münster Electrochemical Energy Technology (MEET), Westfälische Wilhelms-Universität Münster (WWU), Münster, Germany
[2]Faculty of Electrical Engineering and Computer Science, Ingolstadt University of Applied Sciences, Ingolstadt, Germany

Definition and Main Properties

Nonaqueous electrolyte solutions are ion conductors comprising a solvent or blends of solvents and a dissolved salt or several dissolved salts. They may also contain several additives, i.e., materials that improve a wanted property. Due to the huge number of possible solvents, salts, and additives, nonaqueous electrolyte solutions cover large ranges of selectable properties [1]. To give two examples, in comparison to aqueous electrolyte solutions, nonaqueous electrolyte solutions offer wider liquid ranges (down to −150 °C and up to about 300 °C) [2] and an appreciably larger voltage window, also called electro-inactivity range (up to about >4 V vs. about 1.2 V for aqueous systems). Both the large liquid range and the large voltage window not only extend the range of accessible investigations of dissolved materials in fundamental research but offer also applications for processes and in devices that would not be possible with electrolyte aqueous solutions [1].

Properties of nonaqueous electrolyte solutions have been widely studied in fundamental research due to the possibility to vary parameters such as the viscosity and dielectric permittivity of the solvent. The result of these studies mainly conducted in the last century was a better knowledge of spectroscopic and transport properties as well as the thermodynamics of electrolyte solutions [3–17]. The observed behavior was interpreted in terms of structure formation in solutions including solvation of ions, ion pair formation, formation of triple ions and clusters caused by the underlying interactions, the ion/solvent molecule interaction and the ion/ion interaction [2, 5, 6, 9, 14, 18–21].

In applied research the possibility to tailor the properties of the solutions have initiated many applications including processes such as [1, 2, 14, 15]:

- Electroplating of materials that cannot be electroplated from aqueous solutions because hydrogen formation would occur instead, including elements such as Al, Si, Ti, and Dy [22]
- Electrodeposition of nonconducting materials
- Electrosynthesis of organic and inorganic materials
- Deposition of conducting polymers
- Electromachining of metals and alloys.

Nonaqueous electrolyte solutions are also applied in each device that could not work without the large voltage window of these materials, including [23–29, 35–39]:

- Primary lithium cells
- Secondary lithium ion cells and batteries
- Dye sensitized solar cells
- Electrochemical double-layer capacitors.

The last three fields of application are currently under heavy research, development, and marketing worldwide. This statement is especially stressed for secondary lithium-ion cells and batteries that currently are booming. After their successful and increasing use in mobile equipments such as mobile phones, tablet computers, and laptops as well as in electric tools. lithium-ion batteries for battery-electric or hybrid-electric vehicles are beginning to reach the market in large numbers. Electrochemical double-layer capacitors may be useful in addition to lithium-ion batteries when very many cycles at high power densities are requested. Finally, solar cells and also in the future dye sensitized solar cells may be used to produce the electric energy for electric cars that are used for short distances (home to work and back). Finally, secondary lithium-ion batteries of cars can be used to buffer the unsteady delivery of electrical energy from so-called renewable resources.

Solvents

Solvents can be classified according to their properties, including physical properties such as dielectric permittivity, viscosity, and liquid range; chemical properties of the solvent including functional groups of solvent molecules; and physical properties of isolated solvent molecules, such as dipole moment and polarizability and last but not least empirical solvent parameters [1, 2]. Empirical solvent parameters can be obtained by measuring the interaction of the studied solvent molecule with other molecules. For example, Gutmann's donor number (DN) obtained by reaction enthalpy measurements of dissolved solvent molecules with the Lewis acid $SbCl_5$ is an excellent measure of the Lewis basicity of a solvent and hence its ability to solvate cations. The acceptor number (AN) scale reflects the Lewis acidity of the solvent and is measured by ^{31}P NMR chemical shift measurements of the strong base triethylphosphine oxide reflecting the ability of a solvent molecule to solvate anions. Other important empirical parameters include solvatochromic parameters including Kamlet and Taft's α-, β-, and π^* scales that are related to the ability to accept or donate hydrogen bonds and to the polarity and polarizability of a solvent. Dimroth and Reichardt's E_T (30) scale is a useful measure for the polarity (ionizing power) of a solvent as well. These solvatochromic parameters are spectroscopically determined by measuring the interaction of a solvent molecule with a selected dye. For details and references to original papers, see [1, 2, 18]. Based on those aforementioned criteria and solvent classes proposed

by other workers, we [1] proposed to classify solvents according to eight classes, including:

1. Amphiprotic hydroxylic solvents, typical examples are the alcohols
2. Amphiprotic protogenic solvents, e.g., carboxylic acids
3. Protophilic H-bond donor solvents, e.g., amines
4. Dipolar aprotic protophilic solvents, e.g., pyridine
5. Dipolar aprotic protophobic solvents, e.g. esters
6. Low-permittivity electron donor solvents, e.g. ethers
7. Low polarity solvents of high polarizability, e.g. benzene
8. Inert solvents, e.g. alkanes and perfluoroalkanes.

For tables of solvents of these classes including physical properties (melting point, boiling point, dielectric permittivity, viscosity, density, dipole moment, and the mentioned empirical solvent parameters), see Ref. [1]. These and similar tables can also be found in Refs. [8, 14, 15, 18]. Suffice it to state here that selected solvents and solvent blends of classes 5 and 6 are often used in practical applications due to their superior electrochemical stability.

Salts

Generally, in nearly every publication devoted primarily to electrolyte solutions apart from solvents, the role of ions is taken into account as well, especially when solvent molecule–ion interaction (solvation) is considered. Marcus has published a review book [19] including several aspects of electrolyte solutions seen from the ion's side including topics such as ionic radii, partial molar quantities, ionic volumes, polarizability, and ionic transport. In contrast to the last century, where mainly salts consisting of atomic ions have been studied currently, molecular organic ions are gaining increasing interest. This statement is especially true for ionic liquids and their solutions in organic solvents consisting of both molecular organic cations and anions. It holds also for large molecular anions bearing many electron-withdrawing substituents, i.e., the so-called weakly coordinating anions that show apart from fascinating properties also many possible applications [23]. Some of the corresponding acids of these anions are very strong acids and may even reach the state of superacids. Whereas the role of specific ion effects is a mature field of research for aqueous solutions [30], it has rarely been studied for nonaqueous solutions. Another field of current interest is the supermolecular chemistry of anions [20] that focuses on anionic coordination chemistry and theoretical and practical aspects of anion complexation. An example from electrolyte research for lithium-ion cells may be appropriate here. It is well known that LiF is scarcely soluble in any solvent. However, it is possible to obtain highly conducting LiF solutions in nonaqueous solvents by means of anion receptors based on boron, such as tris(pentafluorophenyl) borane [31, 32], increasing the solubility of the nearly insoluble salt LiF by six orders of magnitude up to 1 $mol \cdot L^{-1}$ solutions.

Additives

Generally, every application of nonaqueous electrolyte solutions needs its specific additives to prevent problems in the intended application or to increase the shelf life of a device or a process. For example, in lithium-ion batteries there are several critical processes that decide on its shelf life. According to their role the following additives are used to reach this requirement: solid electrolyte interphase forming improvers, cathode protecting agents, overcharge protecting agents, wetting agents, flame retardant agents, and Al-current-collector corrosion inhibitors. For recent reviews see [33, 34].

Future Directions

The future of this research field is extremely bright. The meaning of the title of a review written nearly 20 years ago still holds: *Solution chemistry: A cutting edge in modern electrochemical technology* [1]. Driven by the economic interest research efforts will continue and will be expanded. Despite the fact that electrolyte solutions are under investigation since more than 100 years, several interesting topics related

to fundamental research are not yet understood. To give an example, up to now we are waiting for a useful theory that is able to calculate transport properties of nonaqueous electrolyte solutions starting from quantum-mechanical levels. Also the role of ion pairs and higher clusters is not completely understood and invites workers for further research. To give an example, charge transport in electrolytes of low dielectric permittivity (including solid polymer electrolytes and gels) in lithium-ion cells may be based on transport of ion pairs instead of lithium-ion transport. A combined research program including spectroscopic (such as dielectric permittivity studies and infrared spectroscopy studies) and electrochemical studies is needed to resolve these open questions. A final cautionary statement is stressed here again: Many workers that are not familiar with nonaqueous systems are not aware of the fact that water affects the results of measurements directly (e.g., by hydrolysis of constituents of the solutions) and indirectly by changing the coupled equilibria governing the properties of electrolyte solutions, especially when the concentrations of the salts are low. We observed changes of > 100 % for 0.1 % water content and repeated a diffusion measurement at thin layer cells ($\sim$30 μm thickness) without protecting inert atmosphere and received doubled diffusion coefficients despite rather short times where the non-dried cells were in contact with the atmosphere. To sum up, working with nonaqueous electrolyte solutions means strictly controlling the water content be Karl–Fischer titration or other useful methods and working under controlled pure inert gas.

Cross-References

- ▶ Conductivity of Electrolytes
- ▶ Electrolytes for Electrochemical Double Layer Capacitors
- ▶ Electrolytes for Rechargeable Batteries
- ▶ Ion Mobilities
- ▶ Ion Properties
- ▶ Ionic Liquids

References

1. Barthel J, Gores HJ (1994) Chap 1. Solution chemistry: a cutting edge in modern electrochemical technology. In: Mamontov G, Popov AI (eds) Chemistry of nonaqueous electrolyte solutions. Current progress. VCH, New York, pp 1–148
2. Gores HJ, Barthel J, Zugmann S, Moosbauer D, Amereller M, Hartl R, Maurer A (2011) Chap. 17. Liquid nonaqueous electrolytes. In: Daniel C (ed) Handbook of battery materials, 2nd edn. Wiley-VCH, Weinheim, pp 525–626
3. Robinson RA, Stokes RH (1959) Electrolyte solutions, 2 revth edn. Butterworth, London (Reprint 2003, Dover Publications, New York)
4. Harned HS, Owen BB (1958) The physical chemistry of electrolyte solutions, 3rd edn. Reinhold, New York
5. Gurney RW (1953) Ionic processes in solution. McGraw-Hill, New York
6. Gurney RW (1962) Ions in solution. Dover Publications, New York (reprint)
7. Barthel J (1976) Ionen in nichtwäßrigen Elektrolytlösungen. Dr. D. Steinkopff, Darmstadt
8. Barthel J, Krienke H, Kunz W (1998) Physical chemistry of electrolyte solutions, modern aspects, vol 5. Dr. Dietrich Steinkopff Verlag GmbH & Co. KG, Darmstadt
9. Bockris JO'M, Reddy AKN (1998) Modern electrochemistry, vol. 1: ionics, vol 2. Plenum Press, New York
10. Luckas M, Krissmann J (2001) Thermodynamik der Elektrolytlösungen. Springer, Berlin
11. Lee LL (2008) Molecular thermodynamics of electrolyte solutions. World Scientific Publishing, Singapore
12. Falkenhagen H (1971) Theorie der Elektrolyte. S. Hirzel, Leipzig
13. Friedman HL (1962) Ionic solution theory based on cluster expansion methods, vol 3, Monographs in statistical physics. Wiley, New York
14. Izutsu K (2009) Electrochemistry in nonaqueous solutions, 2nd edn. Wiley-VCH, Weinheim
15. Aurbach D (1999) Nonaqueous electrochemistry. Marcel Dekker, New York
16. Mann CK (1969) Nonaqueous solvents for electrochemical use in electroanalytical chemistry. In: Bard AJ (ed) Electroanalytical chemistry, vol 3. Marcel Dekker, New York, p 57
17. Marcus Y (1977) Introduction to liquid state chemistry. Wiley, London
18. Marcus Y (1985) Ion solvation. Wiley, Chichester
19. Marcus Y (1997) Ion properties. Marcel Dekker, New York
20. Bianchi A, Bowman-James K, Enrique García-España E (1997) Supramolecular chemistry of anions. Wiley-VCH, Weinheim
21. Marcus Y, Hefter GT (2006) Ion pairing. Chem Rev 106(11):4585–4621
22. Lodermeyer J, Multerer M, Zistler M, Jordan S, Gores HJ, Kipferl W, Diaconu E, Sperl M,

Bayreuther G (2006) Electroplating of dysprosium, electrochemical investigations, and study of magnetic properties. J Electrochem Soc 153(4): C242–C248
23. Nakajima T, Groult H (eds) (2005) Fluorinated materials for energy conversion. Elsevier, Amsterdam
24. Xu K (2004) Nonaqueous liquid electrolytes for lithium-based rechargeable batteries. Chem Rev 104:4303–4418
25. Barthel J, Gores HJ, Schmeer G, Wachter R (1983) Nonaqueous electrolyte solutions in chemistry and technology. Top Curr Chem 111:33
26. von Schalkwijk W, Scrosati B (eds) (2002) Advances in lithium-ion batteries. Kluwer, New York
27. Yamamoto O, Wakihara M (1998) Lithium-ion batteries. Wiley-VCH, Weinheim
28. Yoshio M, Brodd RJ, Kozawa A (eds) (2003) Lithium ion batteries. Springer, New York
29. Nazri GA, Pistoia G (2003) Lithium batteries, science and technology. Springer, New York (first softcover printing 2009)
30. Kunz W (ed) (2010) Specific ion effects. World Scientific, New Jersey
31. McBreen J, Lee HS, Yang XQ, Sun X (2000) New approaches to the design of polymer and liquid electrolytes for lithium batteries. J Power Sources 89:163–167
32. Lee HS, Yang XQ, Sun X, McBreen J (2001) Synthesis of a new family of fluorinated boronate compounds as anion receptors and studies of their use as additives in lithium battery electrolytes. J Power Sources 97–98:566–569
33. Ue M (2003) Chap. 4. Role-assigned electrolytes: additives. In: Yoshio M, Brodd RJ, Kozawa A (eds) Lithium ion batteries. Springer, New York, pp 75–115
34. Zhang SS (2006) A review on electrolyte additives for lithium-ion batteries. J Power Sources 162:1379–1394
35. Linden DE, Reddy TB (2002) Handbook of batteries, 3rd edn. McGraw-Hill, New York
36. Winter M, Brodd RJ (2004) What are batteries, fuel cells, and supercapacitors? Chem Rev 104(10):4245–4270
37. Conway BE (1999) Electrochemical supercapacitors. Kluwer, New York
38. O'Reagan B, Grätzel M (1991) A low-cost, high-efficiency solar cell based on dye-sentizied colloidal TiO_2 films. Nature 353:737
39. Hinsch A, Behrens S, Berginc M, Boennemann H, Brandt H, Drewitz A, Einsele F, Fassler D, Gerhard D, Gores H, Haag R, Herzig T, Himmler S, Khelashvili G, Koch D, Nazmutdinova G, Opara-Krasovec U, Putyra P, Rau U, Sastrawan R, Schauer T, Schreiner C, Sensfuss S, Siegers C, Skupien K, Wachter P, Walter J, Wasserscheid P, Wuerfel U, Zistler M (2008) Material development for dye solar modules: results from an integrated approach. Prog Photovoltaics 16(6):489–501

Non-Faradaic Electrochemical Modification of Catalytic Activity (NEMCA)

Tatsumi Ishihara
Department of Applied Chemistry, Faculty of Engineering, International Institute for Carbon Neutral Energy Research(WPI-I2CNER), Kyushu University, Nishi-ku, Fukuoka, Japan

Introduction

One of the useful applications of a solid electrolyte is a convertor from chemical energy to electricity (fuel cell) or from chemicals to another useful compound (ceramic reactor). In particular, application of solid electrolyte for so-called electrochemical ceramic reactor is highly attracting because of a selective conversion achieved. In the ceramic reactor, ion species are supplied through electrolyte to the electrode catalyst electrochemically, and so, conversion of reactant to the objective products is performed by using the permeated ion species as a reactant. Therefore, the formation rate of reaction products is generally the same or of lower amount than that of pumped ion species. Namely, formation rate of products should obey the Faraday's law. However, in 1981, interesting phenomena were first reported by Vayenas et al. in the high-temperature electrochemical reactor, and they found that the catalytic activity and selectivity depended strongly on the catalyst potential and the electrochemically induced reversible change in the catalytic rate was found to exceed the rate of ion pumping to the catalyst by up to five orders of magnitude and thus the rate change does not obey the Faraday's law [1]: Since the improvement in catalytic activity does not obey the Faraday's law, this improvement in catalytic reaction rate under a condition of electrochemically pumping ions, typically, oxide ion or Na^+, is called "non-Faradaic electrochemical modification of catalytic activity process (NEMCA)" [2] or electrochemical promotion of catalysis

(EPOC) [3]. Here, unique effects of NEMCA or EPOC effects are explained briefly.

EMCA (or EPOC) Effects on Catalysis

The basic concept of this NEMCA or EPOC is shown in Fig. 1 where O^{2-} conducting solid electrolytes is used for C_2H_4 oxidation [4]. The porous metal catalyst electrode, typically 0.05–2 μm thickness, is deposited on the solid electrolyte and under open-circuit conditions, i.e., $I = 0$, no electrochemical pumping oxygen; no product forms in C_2H_4 oxidation as shown in Fig. 1. Application of an electrical current I of 1 mA or potential of 0.5 V between the Pt catalyst and a counter electrode causes significant influence. The catalytic rate increase (Δr) is 25 times larger than the rate r_0 before current application and 74,000 times larger than the rate I/2 F of O^{2-} supply to the catalyst electrode.

Similar improvement in non-Faradaic improvement in electrochemical reaction is also reported for various reactions not only for partial oxidation with oxide ionic conductor but also for hydrogenation reaction with proton conductor, or NO reduction with CO on Na^+ ion conductor [3]. Until recently [5], more than 70 different catalytic reactions, i.e., oxidations, hydrogenations, dehydrogenations, isomerizations, and decompositions, have been electrochemically promoted on Pt, Pd, Rh, Ag, Au, Ni, IrO_2, and RuO_2 catalysts deposited on ionic conductor of O^{2-} (Y_2O_3 stabilized ZrO_2, YSZ), Na^+ (β-Al_2O_3); H^+ ($CaZr_{0.9}In_{0.1}O_3$, Nafion); F^- (CaF_2); aqueous, molten salt; and mixed ionic-electronic (TiO_2, CeO_2) conductors. Table 1 summarizes the reaction and ionic conductor reported for NEMCA. Clearly NEMCA is not limited to any particular class of conductive catalyst, catalytic reaction, or ionic conducting support.

Two parameters Λ and ρ are commonly used to describe the magnitude of NEMCA effects:

1. The apparent Faradaic efficiency, Λ:

$$\Lambda = \Delta r_{catalytic}/(I/nF)$$

where $\Delta r_{catalytic}$ is the current or potential induced change in catalytic rate, I is the applied current, n is the charge of the applied ion, and F is the Faraday's constant.

2. The rate enhancement, ρ:

$$\rho = r/ro$$

where r is the electro-promoted catalytic rate and ro is the un-promoted (open-circuit) catalytic rate.

3. The promotion index, PI_j, where j is the promoting ion (e.g., O^{2-} for the case of YSZ or H^+ for the case of Nafion), defined from:

$$PI_j = (\Delta r/\Delta r_0)/\Delta\theta_j$$

where θ_j is a coverage of the promoting ion on the catalyst surface.

A reaction exhibits electrochemical promotion when $|\Lambda| > 1$, while electrocatalysis is limited to $|\Lambda| < 1$. A reaction is termed electrophobic when $\Lambda > 1$ and electrophilic when $\Lambda < -1$. In the former case, the rate increases with catalyst potential, U, while in the latter case the rate decreases with catalyst potential. Λ values up to 3×10^5 and ρ values up to 150 have been found for several systems. For example, ρ values between 300 and 1,400 have been observed for C_2H_4 and C_3H_8 oxidation on Pt/YSZ, respectively. In the experiment of Fig. 1, $\Lambda = 74{,}000$ and $\rho = 26$, i.e., the rate of C_2H_4 oxidation increases by a factor of 25, while the increase in the rate of O consumption is 74,000 times larger than the rate, I/2 F, of O^{2-} supply to the catalyst [4].

It is reported that not only productivity but also selectivity is affected by NEMCA effects. Figure 2 shows product distribution and current in hydration of electrochemical 1-butene supplied over a dispersed Pd/C catalyst electrode, deposited on Nafion, H^+ conductor at room temperature [6]. Obviously, the products are strongly dependent on the applied potential. The maximum ρ values for the production of *cis*-2-butene, *trans*-2-butene, and butane are of the order of 50, and the corresponding maximum Λ values are of the

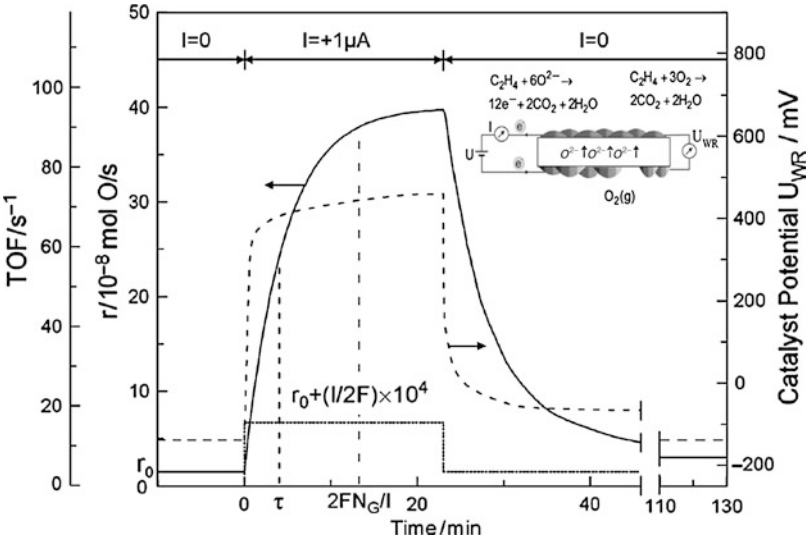

Non-Faradaic Electrochemical Modification of Catalytic Activity (NEMCA), Fig. 1 Basic experimental setup (**a**, **b**). Catalytic rate r and turnover frequency TOF response of C_2H_4 oxidation on Pt deposited on YSZ, an O^{2-} conductor, upon step changes in applied current (T = 643 K, P_{O2} = 4.6 kPa, P_{C2H2} = 0.36 kPa)

Non-Faradaic Electrochemical Modification of Catalytic Activity (NEMCA), Table 1 Typical case of NEMCA effects reported

Reaction	Cell configuration	Pumped oxygen	NEMCA effects	Refs.
C_2H_4, O_2	Pd/YSZ/Au	O^{2-}	Λ values up to 258 and ρ values up to 50	[13]
CO_2, H_2	Pd/β″-Al_2O_3/Au	Na^+	Water-gas shift reaction shows NEMCA effects	[14]
CO_2, H_2	Rh/YSZ/Au	O^{2-}	Formation of CH_4 is promoted by NEMCA effects	[15]
C_2H_4, O_2	Pt/BCN/Au	H^+	Λ values up to 1,000 and ρ values up to 12	[16]
C_2H_5OH, O_2	Pt/YSZ/Pt	O^{2-}	Acetaldehyde and CO_2 production rates are accelerated, Λ values for C_2H_5OH dehydrogenation up to 10^4	[17]
C_3H_6, O_2	LSCM/YSZ/Pt	O^{2-}	LSCM is restricted to oxidizing atmosphere	[18]
C_3H_6,O_2	Pt/β″-Al_2O_3/Au	K^+	ρ values up to 6	[19]
C_3H_6, O_2	Pt/NASICON/Au	Na^+	ρ values values up to 3 close to stoichiometric	[20]
C_3H_8, O_2,	Pt/β″-Al_2O_3/Au	Na^+	Changes in catalytic rate larger than 60 times than corresponding changes in sodium coverage	[21]
NO,O_2, C_3H_6	Ir/YSZ	O^{2-}	Increase in N_2 selectivity upon positive applied current	[22]
NH_3	Ru/SCY/Ag	H^+	75 % decrease in the reaction activation energy under positive polarization	[23]
C_3H_6, H_2O	Pd/SCY/Pd	H^+	4-fold increase in the rate of propane decomposition. During the electrochemical pumping of hydrogen, the rate of hydrogen pumped to the outer chamber over I/2F reaches values up to 0.9	[24]

order of 40 for *cis*-2-butene formation, 10 for *trans*-2-butene formation, and less than one for butane formation. Thus, each proton supplied to the Pd catalyst can cause the isomerization of up to 40 1-butene molecules to *cis*-2-butene and up to 10 1-butene molecules to *trans*-2-butene, while the hydrogenation of 1-butene to butane is electrocatalytic, i.e., Faradaic reaction. Therefore, this non-Faradaic activation of heterogeneous catalytic reactions is a novel

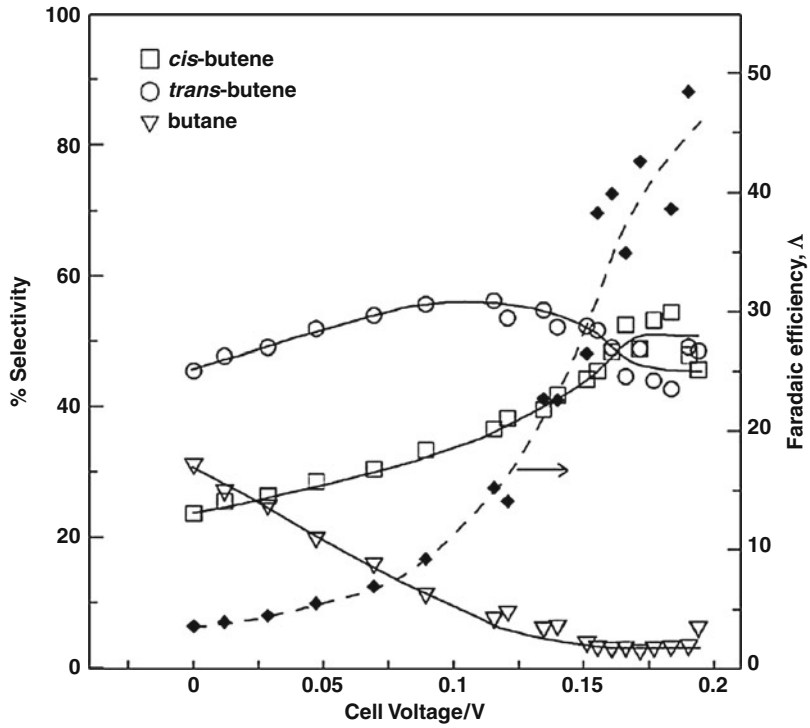

Non-Faradaic Electrochemical Modification of Catalytic Activity (NEMCA), Fig. 2 Product distribution and current in hydration of electrochemical 1-butene supplied over a dispersed Pd/C catalyst electrode, deposited on Nafion

application of electrochemistry with several technological possibilities, particularly in useful product selectivity modification and in exhaust gas treatment.

Mechanism for NEMCA Effects

The origin of NEMCA effects is also studied, and it is reported that the surface modification of reactant by ion back spillover of an effective double layer at the metal-gas interface is strongly related with unique improvement in reaction rate and selectivity [5, 7]. In situ work function measurements are performed by the Kelvin probe technique [7] or UPS [8] for explanation of NEMCA effects. These measurements show that over a wide range of temperatures, work function of metal catalyst linearly changes with increasing potential and the supplied ion species like oxide ion, proton, or Na^+ spill over [9] on the metal catalyst to form electric double layer. Schematic image of electrochemical modification is shown in Fig. 3 for the case of oxide ion conductor, in which δ value is not still determined yet [5]. Therefore, this electric double layer which forms at the catalyst-gas interface modifies the adsorption state of reactants like oxygen. Change in adsorption state under application of potential is also studied with temperature-programmed desorption [10], X-ray photoelectron spectroscopy [11], etc. Figure 4 shows the typical example of electrochemical modification of oxygen on Pt/YSZ catalyst [5]. In this experiment, desorption of oxygen from gas phase and electrochemically supplied was measured. Figure 4a presents the O_2-TPD spectra on Pt/YSZ when oxygen is supplied from the gas phase. A broad oxygen desorption peak (β2 state) was observed after catalyst exposure to oxygen atmosphere. In Fig. 4b, oxygen has been supplied electrochemically in the form of oxygen ions (O^{2-}) from the support, YSZ, using an external circuit and a constant positive current. Nonstoichiometric oxygen from the support migrates and gets adsorbed on the catalyst surface. O_2-TPD curve consists of one sharp oxygen peak (β3 state) desorbing at higher temperatures than the β2 state. This suggests that the back-spillover oxygen exists and is more strongly adsorbed on the

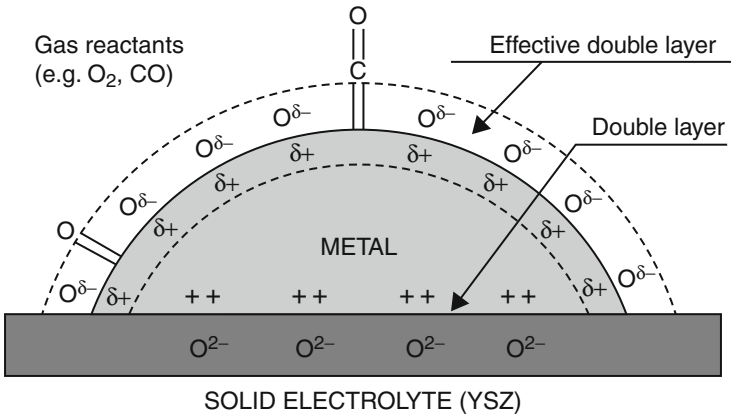

Non-Faradaic Electrochemical Modification of Catalytic Activity (NEMCA), Fig. 3 Schematic image of electrochemical modification

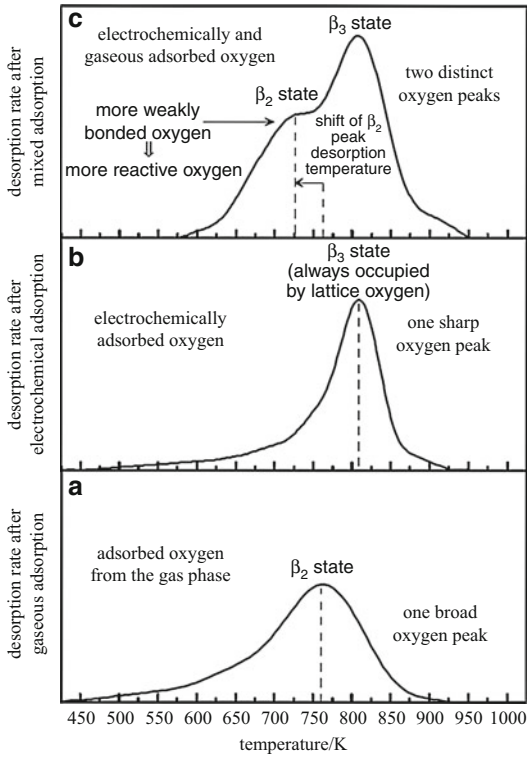

Non-Faradaic Electrochemical Modification of Catalytic Activity (NEMCA), Fig. 4 Typical example of electrochemical modification of oxygen on Pt/YSZ catalyst (**a**) gaseous adsorption, (**b**) electrochemical adsorption, and (**c**) mixed adsorption [5]

surface than the gaseous oxygen of β2 state. Figure 4c is the O_2-desorption under gas-phase adsorption and oxygen-pumping condition, namely, a mixed adsorption condition. Two oxygen peaks evidently appear, a broad one originating from the gas phase (β2 state) and a sharper one (β3 state) occupied by a more strongly bonded oxygen. It is worth noting that the β3 state which corresponds to the back-spillover oxygen species acts as a promoter for supplied oxygen since the last one moves to more weakly bonded states on the catalyst surface (lower desorption temperatures). Using ^{18}O tracer adsorption experiment, these weakly desorbed species are recombination ones of oxygen from gas phase and electrochemically pumped. Consequently, origin of NEMCA or EPOC effects could be assigned to such significant improvement in reactivity of adsorbed reactant by contributing the pumped ion species. This is more clearly observed on Na^+- pumping case on CO oxidation [5].

Summary

Many studies have been reported during the last almost 20 years regarding the effect of the electrochemical promotion of catalysis and its origin and application to several types of reactions of environmental and industrial interest. The effectiveness of NEMCA for catalytic oxidations, reductions, hydrogenerations, decompositions, and isomerizations using numerous types of solid electrolytes and catalysts underlines the importance of this phenomenon in both catalysis and electrochemistry. Application of these

effects on the larger size reactor is also studied [12], and this seems to be more popular in the future. In particular, much increase in performance are required for fuel cells and electrocatalytic reactor. Therefore, new concepts based on NEMCA for these area will open a new reseach area.

References

1. Stoukides M, Vayenas CG (1981) The effect of electrochemical oxygen pumping on the rate and selectivity of ethylene oxidation on polycrystalline silver. J Catal 70:137
2. Vayenasa CG, Koutsodontis CG (2008) Non-Faradaic electrochemical activation of catalysis. J Chem Phys 128:182506
3. Katsaounis A (2010) Recent developments and trends in the electrochemical promotion of catalysis (EPOC). J Appl Electrochem 40:885
4. Bebelis S, Vayenas CG (1989) Non-faradaic electrochemical modification of catalytic activity: 1. The case of ethylene oxidation on Pt. J Catal 118:125
5. Vayenas CG, Bebelis S, Pliangos C, Brosda S, Tsiplakides D (2001) Electrochemical activation of catalysis: promotion, electrochemical promotion and metal-support interactions. Kluwer, New York
6. Ploense L, Salazar M, Gurau B, Smotkin ES (1997) Proton spillover promoted isomerization of n-Butylenes on Pd-Black cathodes/nafion 117. J Am Chem Soc 119:11550
7. Vayenas CG, Bebelis S, Ladas S (1990) Dependence of catalytic rates on catalyst work function. Nature (London) 343:625
8. Zipprich W, Wiemhöfer H-D, Vöhrer U, Göpel W (1995) In-situ photoelectron spectroscopy of oxygen electrodes on stabilized zirconia. Ber Bunsenges, Phys Chem 99:1406
9. Harkness I, Lambert RM (1995) Electrochemical promotion of the no + ethylene reaction over platinum. J Catal 152:211
10. Neophytides SG, Vayenas CG (1995) TPD and cyclic voltammetric investigation of the origin of electrochemical promotion in catalysis. J Phys Chem 99:17063
11. Ladas S, Kennou S, Bebelis S, Vayenas CG (1993) Origin of non-faradaic electrochemical modification of catalytic activity. J Phys Chem 97:8845
12. Balomenou S, Tsiplakides D, Katsaounis A, Thiemann-Handler S, Cramer B, Foti G, Comninellis C, Vayenas CG (2001) Novel monolithic electrochemically promoted catalytic reactor for environmentally important reactions. Appl Catal B Environ 52:181
13. Roche V, Karoum R, Billard A, Revel R, Vernoux P (2008) Electrochemical promotion of deep oxidation of methane on Pd/YSZ. J Appl Electrochem 38:1111
14. Bebelis S, Karasali H, Vayenas CG (2008) Electrochemical promotion of the CO2 hydrogenation on Pd/YSZ and Pd/β´´-Al2O3 catalyst-electrodes, Solid State Ionics 179:1391
15. Bebelis S, Karasali H, Vayenas CG (2008) Electrochemical promotion of CO2 hydrogenation on Rh/YSZ electrodes. J Appl Electrochem 38:1127
16. Thursfield A, Brosda S, Pliangos C, Schober T, Vayenas CG (2003) Electrochemical promotion of an oxidation reaction using a proton conductor. Electrochim Acta 48:3779
17. Tsiakaras PE, Douvartzides SL, Demin AK, Sobyanin VA (2002) The oxidation of ethanol over Pt catalyst-electrodes deposited on ZrO2 (8 mol% Y2O3). Solid State Ionics 152:721
18. Gaillard F, Li XG, Uray M, Vernoux P (2004) Electrochemical promotion of propene combustion in air excess on perovskite catalyst. Catal Lett 96:177
19. de Lucas-Consuegra A, Dorado F, Valverde JL, Karoum R, Vernoux P (2007) Low-temperature propene combustion over Pt/K-βAl2O3 electrochemical catalyst: Characterization, catalytic activity measurements, and investigation of the NEMCA effect. J Catal 251:474
20. Vernoux P, Gaillard F, Lopez C, Siebert E (2004) In-situ electrochemical control of the catalytic activity of platinum for the propene oxidation. Solid State Ionics 175:609
21. Kotsionopoulos N, Bebelis S (2007) Top Catal 44:379
22. Vernoux P, Gaillard F, Karoum R, Billard A (2007) Reduction of nitrogen oxides over Ir/YSZ electrochemical catalysts. Appl Catal B Environ 73:73
23. Skodra A, Ouzounidou M, Stoukides M (2006) NH3 decomposition in a single-chamber proton conducting cell. Solid State Ionics 177:2217
24. Karagiannakis G, Kokkofitis C, Zisekas S, Stoukides M (2005) Catalytic and electrocatalytic production of H2 from propane decomposition over Pt and Pd in a proton-conducting membrane-reactor. Catal Today 104:219

Numerical Simulations in Electrochemistry

Bernd Speiser
Institut für Organische Chemie, Universität Tübingen, Tübingen, Germany

Basic Aspects

Simulation is defined as the solution of mathematical equations (mathematical model)

describing a particular physicochemical phenomenon (physical model), here in the electrochemical context. Numerical techniques are commonly involved, because in most cases the mathematical model cannot be solved in a closed form. Since, at present, numerical calculations are almost exclusively performed on digital computers, the term "digital simulation" is also common. Besides experimentation and theoretical description, numerical simulation has been qualified as a third means ("computer experiments") of knowledge generation in science [1].

Electrochemical simulations typically concern phenomena on the levels of (A) complete systems (electrochemical cell including electrodes and electrolyte as well as possibly environment; see, e.g., [2, 3]), (B) transport and reaction close to the electrode [4], or (C) atoms, their bonds and interactions [5]. This essay will be concerned with simulations on intermediate level B.

Owing to the extensive use of computation, numerical simulation is regarded as part of "computational electrochemistry" [6–8], although this term is sometimes restricted to calculations on level (C).

Numerical simulations in electrochemistry are used either in (1) a predictive way, i.e., the results describe a phenomenon which has not (yet) been or even cannot be studied experimentally, or (2) in qualitative (to determine a reaction mechanism) or quantitative (to determine characteristic properties) comparison to experimental data. Often simulation and "modelling" are used as synonyms [9].

Cyclic voltammetry is probably the electrochemical technique that is simulated most often, aiming at the analysis of electrode processes with respect to mechanism, kinetics, and thermodynamics of the reaction steps as well as transport properties of the molecules involved. The simulation of processes at (ultra)microelectrodes is also popular and highly important for the analysis of scanning electrochemical microscopy experiments [10].

For additional information, the reader is referred to earlier reviews on the topic [4, 6, 11–13].

Models

The formulation of physical and subsequently mathematical models is a simplification and abstraction of the complex real processes at the electrode. Thus, for the numerical simulation of electrode reactions, only the most important steps are considered:

- Transport, often restricted to diffusion (Fick's laws), but in principle also including convection (Navier-Stokes equation) and migration (Poisson-Boltzmann equation)
- Electron transfer, most often assumed to follow Butler-Volmer kinetics, but also in Nernstian equilibrium or according to Marcus kinetics
- Adsorption of molecules at the electrode surface, described by isotherms (e.g., Langmuir or Frumkin)
- Preceding or follow-up chemical reactions in the electrolyte phase or on the surface with appropriate kinetics, resulting in the great variety of electrode reaction mechanisms in electroanalytical and electrosynthetic contexts.

The combination of these steps defines the temporal (t) and spatial (for typical one-dimensional models: x; two- and three-dimensional simulations are also performed [10]) variation of the concentrations c of all educts, products, and intermediates involved. The concentrations at the electrode surface and in the bulk of the solution are defined through boundary conditions. Electrode boundary conditions also characterize the type of experiment performed, e.g., a triangular potential variation for cyclic voltammetry or a potential or current step function for chronoampero- or chronopotentiometry, respectively. The equations of the resulting mathematical model form a system of partial differential equations (PDEs) with the c as the unknowns. This system is solved starting from initial values of the unknowns (initial conditions) and subject to the boundary conditions. The primary solution provides concentration profiles $c = f(x)$ as a function of t. The experimental observable (in the case of a potential controlled experiment, the current i through the electrode;

for a current controlled experiment, the potential of the electrode E) is often calculated from these profiles. It may, however, also be considered as an additional unknown [14].

Algorithms

Numerically, the solution of the model equations (PDEs subject to initial and boundary conditions) corresponds to an integration with respect to the space and time coordinates. In general, this is an approximation to the mathematical model's exact solution. In simple cases, often restricted models, *analytical solutions* given by some, even complex, mathematical function are available. Additional work, e.g., Laplace transformation of the original mathematical model, may be required. Generating an analytical solution is commonly not termed simulation ("modelling... without... simulation" [15]). If such solutions are not practical, several techniques are applied, among these:

- *Finite difference approximation* of the concentration profiles. The space and time axes are discretized in the form of points or boxes, and the differential equations are changed into difference equations. The solution reduces to that of a system of ordinary equations.
- *Orthogonal collocation* – the substitution of the concentration profiles by polynomials that are forced to locally fulfil the differential equations exactly at certain points (discretization based on the zeroes of the polynomials). The partial differential equations are reduced to ordinary differential equations to be solved by standard methods.
- *Finite element methods* are based on global constraints imposed on the solution in certain, finite domains ("elements" defining the discretization) along the space coordinate. Thus, the integrated residual between the true and the approximated solutions is forced to zero subject to a weighting function.

Certain electrochemical conditions present problem cases for these algorithms, in particular [11]:

- The development of narrow diffusion layers close to the electrode or reaction fronts inside the electrolyte requires extremely high accuracy in these space regions.
- Abrupt changes in the controlling potential or current cause discontinuous changes of the boundary conditions or concentration profiles with t.
- Fast chemical reaction steps result in "stiff" PDE systems calling for specialized solvers.
- Nonlinearity of mathematical model equations results from reactions with orders higher than unity or particular boundary terms (e.g., adsorption isotherms).

To accommodate such situations, adaptive algorithms have been proposed that dynamically select the discretization step size in t and x according to the situation [16].

Simulators

Algorithms to solve mathematical models in electrochemistry are implemented as computer programs and used in the specific context of a particular experiment, problem, electrode reaction mechanism, etc., to be studied. However, for practical use in the electrochemical community, they have also been generalized in extended program packages (simulators) to be applied to a great variety of situations. Moreover, some electrochemical simulators provide means to easily define reaction mechanisms or experimental details and translate corresponding user input dynamically into the PDE system and its initial and boundary conditions. Finally, tools for data analysis and further tasks may complement a simulator to give a "problem-solving environment" [6].

A selected list of such simulators for electrochemical experiments is given below:

- `cvsim` [17] was an early attempt of a cyclic voltammetry simulator with a fixed selection of common electrode reaction mechanisms. `casim` (for chronoamperometry) and `gesim`

(for galvanostatic electrolyses) were companion programs. Their development (based on orthogonal collocation) has been discontinued.

- `DigiSim` [18] was the first commercialized [19] cyclic voltammetry simulator and remains very popular with a window-based user interface and a rather general input tool for electrode reaction mechanisms, allowing nonprogrammers to formulate the reaction steps in a way intuitive to an electrochemist. It is based on finite difference algorithms.
- `DigiElch` [20] is a rewrite and extension of `DigiSim` with additional features by one of the original authors.
- `ELSIM` [6, 8] uses a somewhat different approach by providing an input tool on the level of the mathematical model which is solved by finite difference techniques.
- `EChem++` [9, 14] is based on adaptive finite elements. Both reaction mechanisms and experimental conditions (such as the potential or current program applied to the electrode as an "excitation" of the electron transfer processes) can flexibly be formulated. It is an open-source program maintaining principles of object-oriented software design [21] and is under continuous development.
- Online simulators have been described [13], but only one (for the specific problem of a monolayer covered electrode order cyclic voltammetric conditions [22]) seems to be working to date [23].

Applications

Simulations are generated in practice in both dimensioned and dimensionless forms. Running a dimensioned simulation requires to know (or assume) real values of parameters describing the modelled system, e.g., rate constants and diffusion coefficients, and leads to results that can directly be compared to experimentally observed currents or potentials.

On the other hand, in dimensionless simulations, all parameters values are normalized. Dimensionless results are particularly valuable because they can be transformed into many real contexts, depending on the normalization equations (usually linear).

It must be noted that, owing to the approximate character of simulations (see above) and the facts that (a) the solutions are not unique (several models may give the same results) and (b) possibly errors in calculation or inadequate model, mathematical, or algorithmic formulations will cancel each other (and consequently go undetected) [1], great care must be taken when drawing conclusions from comparing experiments and simulations [4, 11].

Typical example applications include:

- Simulations are used to explore the behavior of certain mechanisms; see as an example the influence of the attractive or repulsive interaction between molecules (characterized by a_{AB}) upon Frumkin-type adsorption on an electrode surface (Fig. 1) [24].
- A large number of dimensionless simulations can be condensed into working curves or zone diagrams [25].
- (Complex) mechanistic schemes are simulated, and the results are compared to experiments, helping to support or discard mechanistic hypotheses [26]. The example (Fig. 2) shows cyclic voltammograms for a mechanism including 3 electron transfers and 4 chemical steps [27].
- Quantitative comparison between simulation and experiment enables to determine rate constants, redox potentials, and other characteristics of the investigated electrochemical system (see also Fig. 2). In this case, it is strongly advised not to rely on comparison of a single curve but rather to fit simulations to experimental data recorded under widely varying conditions [26].

Conclusions

Numerical simulation is an indispensable tool in electrochemistry to model complex real systems, in particular at the level of chemical reaction and transport processes. The approximation and solution

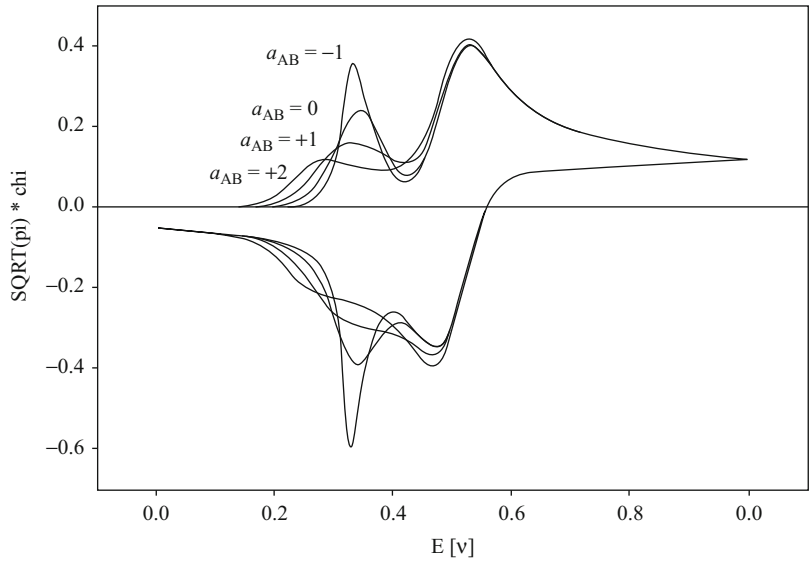

Numerical Simulations in Electrochemistry, Fig. 1 Simulated cyclic voltammograms with dimensionless current ($\pi^{1/2}\,\psi$) for a redox couple with Frumkin adsorption, a_{AB} is the interaction parameter (Adapted from [24])

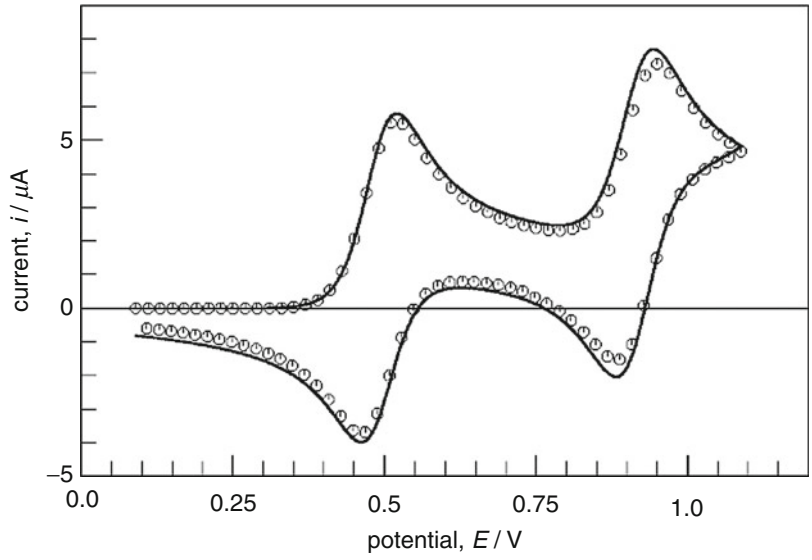

Numerical Simulations in Electrochemistry, Fig. 2 Comparison of simulated (*line*) and experimental (*symbols*) cyclic voltammograms of octamethyl-1,1′-bipyrrole, details, and simulation parameters; see [27] (Adapted from [27])

of partial differential equations that describe the real phenomena lead to an improved understanding of the pertinent reaction mechanisms and their kinetics and thermodynamics. It also allows to determine physicochemical constants and parameters related to the electrochemical process.

Cross-References

► Cyclic Voltammetry

References

1. Heymann M (2006) Understanding and misunderstanding computer simulation: the case of atmospheric and climate science – an introduction. Stud Hist Philos Mod Phys 41:193–200
2. Sorrentino M, Pianese C, Guezennec YG (2008) A hierarchical modeling approach to the simulation and control of planar solid oxide fuel cells. J Power Sources 180:380–392
3. Ramadesigan V, Northrop PWC, De S, Santhanagopalan S, Braatz RD, Subramanian VR (2012) Modeling and simulation of lithium-ion

batteries from a systems engineering perspective. J Electrochem Soc 159:R31–R45
4. Britz D (2003) Digital simulation in electroanalytical chemistry. In: Bard AJ, Stratmann M, Unwin P (eds) Encyclopedia of electrochemistry, vol 3, Instrumentation and electroanalytical chemistry. Weinheim, Wiley-VCH, pp 51–71
5. Jaque P, Marenich AV, Cramer CJ, Truhlar DG (2007) Computational electrochemistry: the aqueous $Ru^{3+}|Ru^{2+}$ reduction potential. J Phys Chem C 111:5783–5799
6. Bieniasz LK (2002) Towards computational electrochemistry – a kineticist's perspective. In: Conway BE, White RE (eds) Mod asp electrochem, vol 19. Marcel Dekker, New York, pp 135–195
7. Gooch KA, Fisher AC (2002) Computational electrochemistry: the simulation of voltammetry under hydrodynamic modulation control. J Phys Chem B 106:10668–10673
8. Bieniasz LK (2007) A unifying view of computational electrochemistry. In: Simons TE, Maroulis G (eds) Computational methods in science and engineering, theory and computation: old problems and new challenges. American Institute of Physics, Melville, pp 481–486
9. Ludwig K, Morales I, Speiser B (2007) EChem++ – an object-oriented problem solving environment for electrochemistry. Part 6. Adaptive finite element simulations of controlled-current electrochemical experiments. J Electroanal Chem 608:102–110
10. Combellas C, Fuchs A, Kanoufi F (2004) Scanning electrochemical microscopy with a band microelectrode: theory and application. Anal Chem 76:3612–3618
11. Speiser B (1996) Numerical simulation of electroanalytical experiments: recent advances in methodology. In: Bard AJ, Rubinstein I (eds) Electroanalytical chemistry, vol 19. Marcel Dekker, New York, pp 1–108
12. Bieniasz LK, Britz D (2004) Recent developments in digital simulation of electroanalytical experiments. Pol J Chem 78:1195–1219
13. Britz D (2005) Digital simulation in electrochemistry. Springer, Heidelberg
14. Ludwig K, Speiser B (2007) EChem++ – an object-oriented problem solving environment for electrochemistry: part 5. A differential-algebraic approach to the error control of adaptive algorithms. J Electroanal Chem 608:91–101
15. Oldham KB, Myland JC (2011) Modelling cyclic voltammetry without digital simulation. Electrochim Acta 56:10612–10625
16. Britz D (2011) The true history of adaptive grids in electrochemical simulation. Electrochim Acta 56:4420–4421
17. Speiser B (1990) EASIEST – a program system for electroanalytical simulation and parameter estimation – I. Simulation of cyclic voltammetric and chronoamperometric experiments. Comput Chem 14:127–140
18. Rudolph M (1995) Digital simulations with the fast implicit finite difference algorithm – the development of a general simulator for electrochemical processes. In: Rubinstein I (ed) Physical electrochemistry. Principles, methods, and applications. Marcel Dekker, New York, pp 81–129
19. Rudolph M, Reddy DP, Feldberg SW (1994) A simulator for cyclic voltammetric responses. Anal Chem 66:589A–600A
20. http://www.elchsoft.com/Default.aspx. Accessed 29 Jun 2013
21. Ludwig K, Rajendran L, Speiser B (2004) EChem++ – an object oriented problem solving environment for electrochemistry. Part 1. A C++ class collection for electrochemical excitation functions. J Electroanal Chem 568:203–214
22. Ohtani M (1999) Quasi-reversible voltammetric response of electrodes coated with electroactive monolayer films. Electrochem Commun 1:488–492
23. Ohtani M. http://www.kanazawa-bidai.ac.jp/~momo/qrcv/QRCV.html. Accessed 29 Jun 2013
24. Schulz C, Speiser B (1993) Electroanalytical simulations. Part 14. Simulation of frumkin-type adsorption processes by orthogonal collocation under cyclic voltammetric conditions. J Electroanal Chem 354:255–271
25. Savéant J-M (2006) Elements of molecular and biomolecular electrochemistry. Wiley, Hoboken
26. Speiser B (2004) Methods to investigate mechanisms of electroorganic reactions. In: Bard AJ, Stratmann M, Schäfer HJ (eds) Encyclopedia of electrochemistry, vol 8, Organic electrochemistry. Wiley-VCH, Weinheim, pp 1–23
27. Kuhn N, Kotowski H, Steimann M, Speiser B, Würde M, Henkel G (2000) Synthesis, oxidation and protonation of octamethyl-1,1′-bipyrrole. J Chem Soc Perkin Trans 2:353–363